Nonmonotonic DNA-length-dependent mobility in pluronic gels

Seungyong You, Ling Wei, Sachin Shanbhag, and David H. Van Winkle

Non-monotonic DNA length-dependent mobility in Pluronic gels

Seungyong You [1], Ling Wei [1], Sachin Shanbhag [2], and David H. Van Winkle [1,*]

[1] Department of Physics, Florida State University, Tallahassee, Florida 32306, United States

[2] Department of Scientific Computing, Florida State University, Tallahassee, Florida 32306, United States

Two-dimensional electrophoresis was used to analyze the mobility of DNA fragments in micellar gels of Pluronic F127 ($EO_{100}PO_{70}EO_{100}$) and Pluronic P123 ($EO_{20}PO_{70}EO_{20}$). The 20 to 3500 base pair DNA fragments were separated by size first in agarose gels, and then in pluronic gels at room temperature. In agarose gels, the DNA mobility decreases monotonically with increasing DNA length. In pluronic gels, however, the mobility varies non-monotonically according to fragment lengths that are strongly correlated with the diameter of the spherical micelles. Brownian dynamics (BD) simulations with short-ranged intra-DNA hydrodynamic interactions (HI) were performed to numerically calculate the length-dependent mobility in pluronic lattices. The rising and falling trends, as well as the oscillations of mobility, were captured by the coarse-grained BD simulations. Molecular dynamics (MD) simulations in pluronic F127, with explicitly modeled micelle coronas, justified that the hydrodynamic interactions mediated by the complex fluid of hydrated poly(ethylene oxide) are a possible reason for the initial rise of mobility with DNA length.

I. INTRODUCTION

Since the pioneering development of the "Tiselius apparatus" for moving boundary electrophoresis by Arne Tiselius [1] in 1937, electrophoresis has steadily evolved into a powerful tool for separation and chemical analysis. Electrophoresis and related techniques have played a pivotal role in the popularity of biochemical methods, such as DNA sequencing [2], blotting [3,4,5], and peptide mass fingerprinting [6-10]. As the materials to be separated and analyzed in physical, chemical and life sciences have become more diverse, some of the focus has shifted towards engineering improved sieving matrices. An understanding of the mechanism driving the separation becomes invaluable as matrices become more complex, allowing us to design, control and optimize macromolecules that are otherwise difficult to separate.

---

[*] Corresponding author: rip@phy.fsu.edu

Specifically, DNA electrophoresis as an analytical technique is routinely used in molecular biochemistry to separate single-stranded or double-stranded DNA fragments by size, conformation or charge. Sieving media used for separations include nanopores [11], surfaces [12], ratchets [13], entropic traps [14,15], magnetic sieves [16], dilute polymer solutions [17], and concentrated polymer gels [18]. Among polymer gels, agarose and polyacrylamide gels are commonly used to separate DNA of size range most often encountered in laboratories. These gels are three-dimensional matrices composed of randomly cross-linked polymers or polymer bundles, with channels and pores through which DNA molecules can pass [19]. However, the pore size in these gels is not uniform; instead, it is broadly distributed [20,21]. This makes it difficult to accurately estimate the characteristic length scale of their internal structures. From a practical standpoint, large pores and broad pore size distribution lower the resolution of separations, which limits applicability to short ssDNA or dsDNA fragments.

Pluronics®, a novel sieving medium with distinctly different internal structures from conventional cross-linked polymer gels, have been used to separate biomacromolecules, such as proteins, oligomers and double-stranded DNA, in both capillary [22,23] and conventional electrophoresis [22]. As reported by Rill *et al.* [22], linear, double-stranded DNA up to 3 kbp long can be separated by conventional electrophoresis. Similarly, single-stranded DNA of 4-60 nt long can be separated by capillary electrophoresis. Extraordinary separations of supercoiled DNA are also achieved by capillary electrophoresis [22]. Pluronics are nonionic tri-block copolymers composed of a central poly(propylene oxide) (PPO) block, flanked by a poly(ethylene oxide) (PEO) block on each side. In aqueous solutions, as temperature increases, isolated pluronic unimers self-assemble into spherical micelles, with PPO chains forming micelle cores and PEO chains forming coronas. For some pluronics, at even higher temperatures and (or) by further increasing the polymer concentration, free micelles pack into ordered crystalline structures (gel phases). Figure 1 schematically shows the dependence of structure and morphology on temperature and concentration.
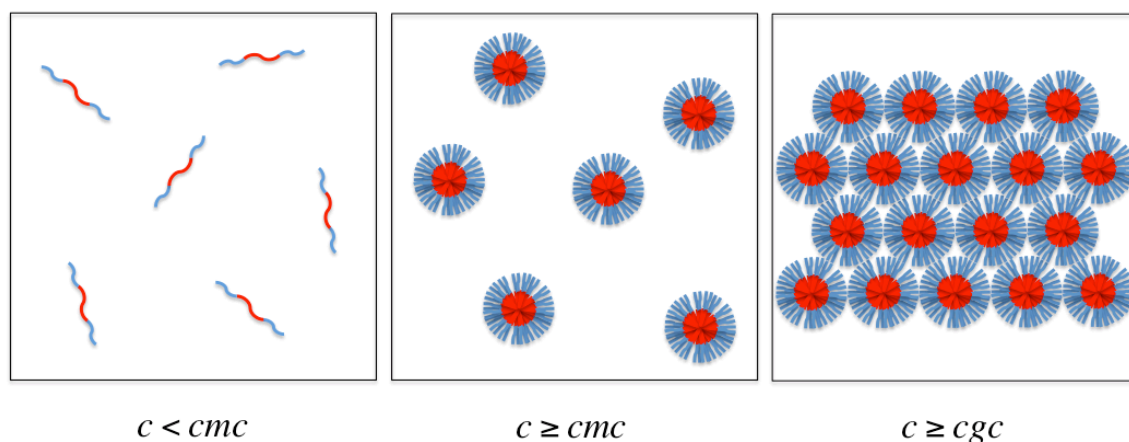

$c < cmc$ $\qquad$ $c \geq cmc$ $\qquad$ $c \geq cgc$

FIG. 1. Schematic illustration of the polymer concentration-dependent structures in aqueous pluronic solutions; cmc, critical micelle concentration; cgc, critical gel concentration; red, PPO; blue, PEO.

You and Van Winkle [24] used single molecule fluorescence microscopy to directly monitor the motion of long DNA molecules (T4-DNA and λ-DNA) undergoing electrophoresis in pluronic F127. Instead of traveling in a reptation mode with extended conformations, sometimes DNA moved as coils, whose radius of gyration was smaller than in free solutions. As reported by You and Van Winkle, both field intensity and gel concentration affected the migration paths of long DNA molecules. At low electric fields and in concentrated gels, DNA traveled along domain boundaries, in a way that was similar to reptation, while DNA migrated through domains along the field direction under strong electric fields and at low gel concentrations. Mechanism of DNA electrophoretic migration in pluronic gels was also studied by linear dichroism spectroscopy. [25,26] At low field strengths, it was shown that DNA in the size range of 200-5400 bp was deformed with the helix axis preferentially perpendicular to the field direction, which supports their hypothesis that DNA migrated along grain boundaries between crystal domains [25,26]. These findings are consistent with the observations by You and Van Winkle under low electric fields.

In the current contribution, electrophoretic migration of short duplex DNA molecules (20-3500 bp) in pluronics F127 and P123 is studied. In random, cross-linked polymer gels, such as agarose or polyacrylamide gels, DNA mobility monotonically decreases with DNA length [27-30, also Appendix A of this contribution]. In contrast, DNA mobility in pluronic gels varies non-monotonically with increasing DNA length. In addition, there is superposed a mobility vs. length modulation corresponding to the micelle diameter. Different from agarose and polyacrylamide gels, pluronic gels have highly ordered internal structures, with well-defined micellar dimensions and micelle packing [23,31-34]. The micelle diameter of pluronics is around 15-20 nm, and the interstitial space between micelles is only a few nanometers [23,31-34]. The stark contrast in internal structures between entangled gels and pluronics strongly suggests that DNA separation mechanisms in these sieving matrices are different.

Classical electrophoresis theories are not able to quantitatively explain the unusual DNA length-dependent mobility in pluronic gels. The dynamics of DNA electrophoresis are complicated; various physical processes are involved [35], including transport through complex geometries, spatial inhomogeneity of the electric field, hydrodynamic interactions, conformational changes, entropic factors, and interactions with surfaces and obstacles. The only practical recourse is to use molecular simulations, which incorporate a subset of these complicated processes, allowing direct comparisons with experimentally measured properties such as DNA mobility. In addition, simulations allow detailed diagnostics that are not achievable in laboratories, providing qualitative insights into molecular processes [35].

Numerical simulations have played an important role in investigating the dynamics of macromolecules in various geometries. Grass *et al.* [36,37] used coarse-grained molecular dynamics simulations to study the dynamic behavior of flexible polyelectrolyte chains, and demonstrated the importance of hydrodynamic interactions during migration in free solutions. Boileau and Slater [38] developed a lattice model to study the low-field gel electrophoresis of short linear or circular oligomers and semi-flexible rods, and showed evidence for entropic effects that could not be captured by the

Ogston model. Laachi *et al.* [39] performed Brownian dynamics simulations on out-of-equilibrium transport of rigid DNA strands in a nanofilter, and predicted that longer DNA molecules traveled faster than shorter ones in periodic arrays of narrow slits and deep wells under strong electric fields, facilitated by the 'torque-assisted escape' during non-equilibrium transport processes. Considerable progress has been made in the understanding of DNA transport in electric fields [40-43] or flows [44,45] through microchannels, obstacle arrays, nanoslits, and other microfluidic devices using Brownian dynamics simulations.

To the best of our knowledge, this is the first computational study of short dsDNA molecules migrating in pluronic liquid crystals subjected to electrostatic driving forces. Understanding the unusual length-dependent mobility, especially the initial rise in mobility with DNA length, is the primary motivation and focus of this contribution. Two hypotheses are proposed to qualitatively explain the initial rise in mobility, namely (i) an entropy driven effect, similar to that observed in liquid chromatography of macromolecules, in which shorter molecules explore smaller pores and take longer to elute than larger molecules; and (ii) hydrodynamic interactions, in which the effective drag per monomer decreases as the chain of monomers gets longer. While the effect of hydrodynamic interaction in free solutions has been well established in both experiments [46] and numerical simulations [36,37], its incorporation and significance in complex geometries are hard to manipulate and poorly understood. In order to test the plausibility of the second hypothesis, Brownian dynamics (BD) simulations with hydrodynamic interactions, which are relatively inexpensive (both in dollars and in time), are performed. As explained later in the paper, the BD simulations support the hydrodynamic interaction based hypothesis. Finally, coarse-grained molecular dynamics simulations are carried out to mechanistically understand the origin of hydrodynamic effect in BD simulations, and rule out the chromatographic effect hypothesis.

II. MATERIALS AND METHODS

A. Materials

Agarose 1000 and agarose were purchased from Invitrogen (Carlsbad, CA), and SeaKem LE agarose was purchased from Cambrex (Rockland, ME). Commercial pluronics F127 and P123 were purchased from BASF (Mount Olive, NJ) and Sigma-Aldrich (St. Louis, MO), respectively. Tris (base) was purchased from Avantor (Center Valley, PA), boric acid from Fisher Scientific (Fair Lawn, NJ), and ethylenediaminetetraacetic acid from Sigma-Aldrich (St. Louis, MO). All the polymers and buffer reagents were used without further purification. All the solutions were prepared in ultrapure water from arium 611VF laboratory water purification system (Sartorius, Edgewood, NY). Agarose was dissolved in 1×TBE buffer (89 mM Tris base, 89 mM boric acid, 2 mM EDTA, pH 8.2-8.4) and stored in a 65°C water bath before use. 3% (w/v) agarose 1000 was used for separations of the 10 bp DNA ladder, 3% (w/v) SeaKem LE agarose for the 25 bp DNA ladder, and 1% (w/v) SeaKem LE agarose for the 250 bp DNA ladder. Pluronics were dissolved in 1×TBE buffer in cold room (4°C) and stored in cold room before use. Commercially available 10, 25, 100 and 250 bp dsDNA ladders were used for electrophoresis. The 10 bp DNA ladder (Invitrogen, Carlsbad, CA) consists of 33 ten base pair repeats, from 10 bp to 330 bp. A 25 bp DNA ladder

(Invitrogen, Carlsbad, CA) consists of 18 fragments ranging in length from 25 to 450 bp, at 25 bp increments, plus a 500 bp fragment. Another 25 bp DNA ladder (Promega, Madison, WI) consists of 12 fragments ranging in length from 25 to 300 bp, at 25 bp increments. The 100 bp DNA ladder (Bio-Rad Laboratories, Hercules, CA) consists of 10 fragments ranging from 100 to 1,000 bp at 100 bp increments. The 250 bp DNA ladder (Invitrogen, Carlsbad, CA) was used to obtain the long DNA mobility limit, which consists of DNA fragments ranging from 250 to 3500 bp at 250 bp increments.

For electrophoresis in pluronic F127, all DNA fragments were fluorescently labeled with SYTOX Orange (Molecular Probes, Eugene, OR) at 5:1 ratio of base pairs to dye molecules. Upon binding to nucleic acids, the DNA-SYTOX complex was measured to exhibit about 450-fold fluorescence enhancement from the background of free dyes [13]. The SYTOX Orange has excitation and emission maxima of 547 nm and 570 nm, respectively. For electrophoresis in pluronic P123, all DNA fragments were fluorescently labeled with SYBR Gold (Invitrogen, Carlsbad, CA). The excitation maxima of SYBR Gold for dye-nucleic acid complexes are at ~495 nm and ~300 nm, and emission maximum at ~537 nm. Prior to sample loading, the pre-stained DNA solutions were mixed with bromophenol blue (Sigma-Aldrich, St. Louis, MO), which is conventionally used as gel loading buffer.

B. Electrophoresis

Two-dimensional slab gel electrophoresis was used to analyze the migrating behavior of DNA molecules in pluronic media. 1×TBE buffer was used as running buffer in electrophoresis. 10 bp and 25 bp DNA ladders were first separated individually in agarose gels under a constant DC field. The agarose gel section with the separated bands was cut out and laid horizontally on top of the vertical pluronic gels. The direction of applied electric fields in pluronic gels was thus perpendicular to the separation direction in the agarose gels. An electric field of 6.0 V/cm was applied during the electrophoresis in pluronic gels. The progress of DNA migration in pluronic F127 was monitored by illuminating with a UV lamp (Model C-62, Ultra-violet Products, Inc., San Gabriel, CA) and photographed by a digital camera (EOS Rebel Xsi, Canon, Inc., Japan) every half hour during the electrophoresis. For electrophoresis in pluronic P123, the separated bands were visualized by the dark reader DR46B transilluminator (Clare Chemical Research, Dolores, CO). As shown by Prud'homme, Wu, and Schneider [47], the pluronic micelle structures are quite stable and independent of temperature in the range of 10-75 ºC. So for the current experimental settings, temperature variations due to Joule heating (2-3 degrees above room temperature) will not change the pluronic structures.

The electrophoretic mobility in pluronic gels was determined by the ratio of the average velocity DNA molecules traveled in pluronic gels and the electric field intensity,

$$\mu = \frac{\bar{v}}{E} = \frac{s/t}{E}, \tag{1}$$

where s is the distance DNA migrated along the field direction over a time interval t. The DNA migration distance in pluronic gels was measured after all DNA strands were

transferred into pluronics. By plotting the average intensity profile (ImageJ, National Institutes of Health, Bethesda, MD) of a rectangular region of interest (ROI) enclosing the DNA band, the weighted median value of the intensity histogram was assigned as the band location.

C. Brownian dynamics simulation

1. DNA chains

The discrete wormlike chain model was used to describe the semi-flexible DNA molecules. A DNA fragment was modeled as a string of N identical beads of radius a (each bead representing a 10 bp segment) held together by harmonic bending (U_b) and stretching (U_s) potentials (Fig. 2),
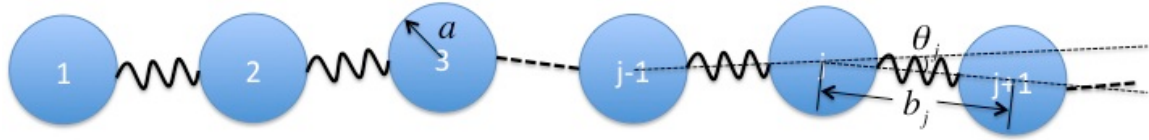

FIG. 2. Schematic illustration of the discrete wormlike chain model.

$$U_b = k_b \sum_{j=1}^{N-2} \theta_j^2 , \qquad (2a)$$

$$U_s = k_s \sum_{j=1}^{N-1} \left(b_j - b \right)^2 , \qquad (2b)$$

where k_b is the force constant for bending, k_s is the force constant for stretching, and b is the equilibrium bead-to-bead distance corresponding to the minimum of the stretching potential. The distance between adjacent beads j and $j+1$ is denoted by b_j; similarly, the angle between adjacent bonds j and $j+1$ is denoted by θ_j.

2. Pluronic matrices

Pluronic gel matrices were modeled as spherical micelles closely packed in face-centered-cubic structures [23,32]. Micelle cores were modeled as impenetrable hard spheres, and reflective boundary conditions were imposed when DNA chains collided with micelle cores. The influence of the structure of micelle coronas on the dynamics of DNA molecules was phenomenologically modeled via four mechanisms: (i) steric repulsion from micelles, (ii) short-ranged intra-DNA hydrodynamic interactions, (iii) long-ranged screening of hydrodynamic coupling [48] due to the PEO hairs, and (iv) increased friction for longer DNA molecules due to entanglement with the PEO polymers. It has been verified (Results and Discussion) that all these mechanisms are essential to describe DNA migration in pluronic lattices, and collectively lead to qualitative agreement with experimental measurements.

Due to the brush-like structure of micelle coronas, DNA molecules are repelled from regions of high EO polymer density in the vicinity of micelle cores. Therefore, a linear repulsive force ($\vec{F}_{re}$) centered at micelle cores is applied on individual DNA segments to account for the steric repulsion within the corona regions,

$$\vec{F}_{re}(r) = \begin{cases} k\dfrac{R_m - r}{R_m - R_c}\hat{r}, R_c < r < R_m \\ 0, otherwise \end{cases}, \tag{3}$$

where r is the distance of a DNA segment from the closest micelle center, $\hat{r}$ is the unit vector from the center of the closest micelle to the DNA segment, R_m and R_c are the radii of micelles and micelle cores, respectively, and k is the repulsive force constant.

The standard methods of incorporating hydrodynamic interactions [49] are not applicable to the pluronic systems, in consideration of the complex geometries as well as the non-dilute polymer regime in pluronic gels. Instead, the hydrodynamic interactions were modeled by the configuration-dependent hydrodynamic interaction tensor ($\overset{\leftrightarrow}{D}$),

$$\overset{\leftrightarrow}{D}_{ii} = \begin{cases} \dfrac{1}{6\pi\eta a}\overset{\leftrightarrow}{I}, L < l_e \\ \dfrac{l_e}{L}\dfrac{1}{6\pi\eta a}\overset{\leftrightarrow}{I}, L \geq l_e \end{cases}, \tag{4a}$$

$$\overset{\leftrightarrow}{D}_{ij} = \begin{cases} \dfrac{1 - \tanh\left(\dfrac{r_{ij}}{b} - \dfrac{l_{HI}}{b}\right)}{1 - \tanh\left(-\dfrac{l_{HI}}{b}\right)}\dfrac{1}{6\pi\eta r_{ij}}\overset{\leftrightarrow}{I}, L < l_e \\ \dfrac{1 - \tanh\left(\dfrac{r_{ij}}{b} - \dfrac{l_{HI}}{b}\right)}{1 - \tanh\left(-\dfrac{l_{HI}}{b}\right)}\dfrac{l_e}{L}\dfrac{1}{6\pi\eta r_{ij}}\overset{\leftrightarrow}{I}, L \geq l_e \end{cases} \quad i \neq j, \tag{4b}$$

where η is the (homogeneous) viscosity inside the matrix, r_{ij} is the distance between ith and jth beads, and $\overset{\leftrightarrow}{I}$ is a 3×3 identity tensor. The diagonal blocks of $\overset{\leftrightarrow}{D}$ are self-diffusion coefficients of individual beads, and off-diagonal blocks describe the pair-wise intra-chain hydrodynamic interactions. Entanglement of long DNA molecules with PEO polymers was modeled according to the transition from the Rouse to the reptation model [50], where the DNA diffusivity is reduced by a factor of $1/L$ (L is the contour length of the DNA molecule). The entanglement length was chosen as $l_e = 10b$ for both pluronics

in the following Brownian dynamics simulations, in consideration of the characteristic length scale of the micelle close-packed crystal structures. A cutoff length l_{HI} was prescribed as the threshold beyond which hydrodynamic interactions is screened. The cutoff boundary was made soft by replacing the sharp step function by a hyperbolic tangent function. $l_{HI} = 10b$ was used in the current Brownian dynamics studies.

3. Electrostatic potential

Finite Difference Method (FDM) was used to numerically solve the Poisson's equation, subject to Dirichlet boundary conditions in the external field direction and periodic boundary conditions in the other two directions. The relative permittivity ε was assumed to be different, but uniform within respective micelle core and corona regions. It was estimated from the volume fraction of poly(propylene oxide) ($\varepsilon_{PO} = 4.9$) and poly(ethylene oxide) ($\varepsilon_{EO} = 4.5$) polymers in corresponding regions. The relative permittivity in the interstitial space was set to be the same as the permittivity of water ($\varepsilon_{H_2O} = 80$). The electrostatic potential is fairly uniform in the plane perpendicular to the field direction (data not shown). This is not surprising, since the electric permittivity is dominated by water, and is practically homogeneous.

4. Dynamics

The Brownian dynamics algorithm of Ermak and McCammon [51] was used to compute the time evolution. Let $\vec{r}_i^{\,0}$ denote the position of bead i at the start of a dynamics step of duration Δt, then, its position after Δt is given by

$$\vec{r}_i = \vec{r}_i^{\,0} + \Delta t \sum_{j=1}^{N} \overleftrightarrow{D}_{ij}^{\,0} \cdot \vec{F}_j^{\,0} + \vec{R}_i(\Delta t), \qquad (5a)$$

where $\vec{F}_j^{\,0}$ is the initial direct force on bead j, and $\vec{R}_i(\Delta t)$ is a random displacement with Gaussian distribution and satisfies

$$\left\langle \vec{R}_i(\Delta t) \right\rangle = 0, \qquad (5b)$$

$$\left\langle \vec{R}_i(\Delta t) \vec{R}_j(\Delta t) \right\rangle = 2 \overleftrightarrow{D}_{ij}^{\,0} \Delta t. \qquad (5c)$$

$\vec{R}_i(\Delta t)$ is calculated from a weighted sum of the normal random deviates [51],

$$\vec{R}_i(\Delta t) = \sum_{j=1}^{i} \overleftrightarrow{\sigma}_{ij} \vec{X}_j, \qquad (5d)$$

with the weighting factors given by

$$\overset{\leftrightarrow}{\sigma}_{ii} = \left(\overset{\leftrightarrow}{D}_{ii} - \sum_{k=1}^{i-1} \sigma_{ik}^2 \right)^{1/2}, \tag{5e}$$

$$\overset{\leftrightarrow}{\sigma}_{ij} = \left(\overset{\leftrightarrow}{D}_{ij} - \sum_{k=1}^{j-1} \overset{\leftrightarrow}{\sigma}_{ik} \overset{\leftrightarrow}{\sigma}_{jk} \right) \bigg/ \overset{\leftrightarrow}{\sigma}_{jj}, i > j. \tag{5f}$$

The modified hydrodynamic interaction tensor is not guaranteed to be positive-semi-definite for all chain configurations; therefore pre-averaging of the tensor obtained from an ensemble average of configurations (under zero electric field) was carried out before running the Brownian dynamics simulations. This approximation also mitigates the computational cost of the algorithm of Ermak and McCammon [51] ($t \propto N^3$). In a single run, the center of mass of a DNA molecule was allowed to traverse through 300 unit cells along the field direction. The first one third of the trajectory was used to equilibrate the system, and the remaining two thirds was used to compute the electrophoretic mobility. The mean mobility of a DNA chain was calculated by averaging over 50 independent runs at each parameter setting.

III. RESULTS AND DISCUSSION

A. Electrophoretic mobility in pluronic gels

Figure 3 shows the 2DE result of the 25 bp DNA ladder moving from left to right under electrophoresis in 22% pluronic F127 gel. The first column shows that DNA bands have been pre-separated from top to bottom in an agarose gel. In the second column, all the DNA bands have entirely moved from the agarose gel into the pluronic gel. At this early time, short DNA bands remain compact while long DNA bands become extended. This effect occurred at the agarose-pluronic interface and appeared in all concentrations. This is because small DNA fragments move faster in agarose gels than in pluronic gels, while large DNA fragments move faster in pluronic gels than in agarose gels.
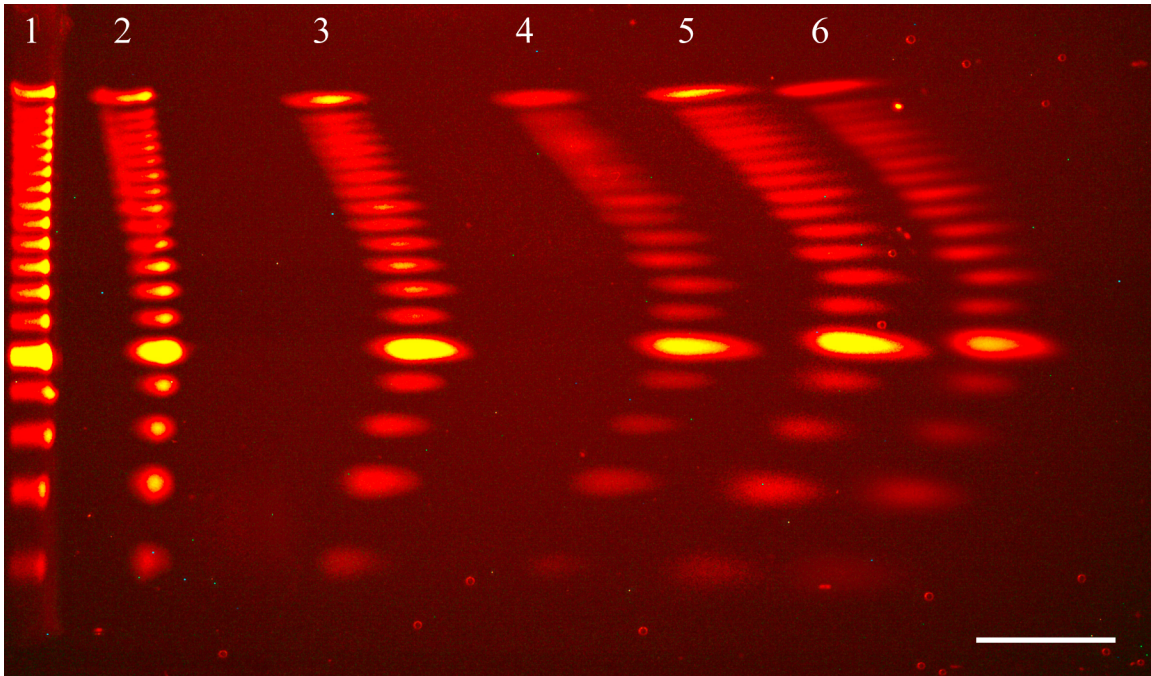
FIG. 3. The 2DE result of the 25 bp DNA ladder progressing from left to right in 22% pluronic F127. DNA bands are distributed from bottom to top of each column; from 25 to 450 bp at 25 bp increments, plus a 500 bp fragment, where 125 and 500 bp fragments are 2 - 3 times brighter than the others by manufacturer design. The left-most (first) column shows the initial status of the DNA bands separated by size in 3% agarose gel. The DNA bands moved through the pluronic gel from the second column to the sixth column. The scale bar is 1 cm in length.

From the second to the sixth columns, it is obvious that small DNA fragments (< 125 bp) become faster but large DNA fragments (> 175 bp) become slower as the molecular size increases. The 25 bp band has about the same mobility as the 450 bp band. The bandwidth increases 2-3 times during the course of the experiment, and its spreading is less in higher concentrations of pluronic gels. In low concentrations (18 or 20 %), however, short DNA fragments (< 100 bp) significantly diffuse and become unobservable after several hours. An erratic zig-zag pattern forms at the leading edge and appears in all concentrations of pluronic F127 gels. The 125, 175, and 225 bands are relatively faster, and the 150, 200, and 250 bands are relatively slower. The zig-zag pattern persists no matter where the bands are located, either in the center or on the side of the gels (data not shown). It is conceivable that this zig-zag effect could be due to sequence effects. As one test of this we repeated the 2DE experiment with another 25 bp DNA ladder from a different manufacturer, Promega (Madison, WI).

Figure 4 shows the 2DE separation of the mixture of the 25 bp DNA ladder (Promega, Madison, WI) and the 100 bp DNA ladder in 24% pluronic F127 gel. The first column shows the initial state of the separated ladders in agarose gel, and the second column was taken when all bands had entirely moved from the agarose gel into the pluronic gel. The smallest fragment is 50 bp as shown in the lowest edge of the first column. As the DNA molecules travel through the medium, the 125 bp and 175 bp bands

move the fastest. Obviously, the DNA molecules shorter than 125 bp and longer than 175 bp are slower. The zig-zag pattern dominates at the sixth column, where the 125, 175, and 225 bands form peaks, and the 150, 200, and 250 bands form troughs.
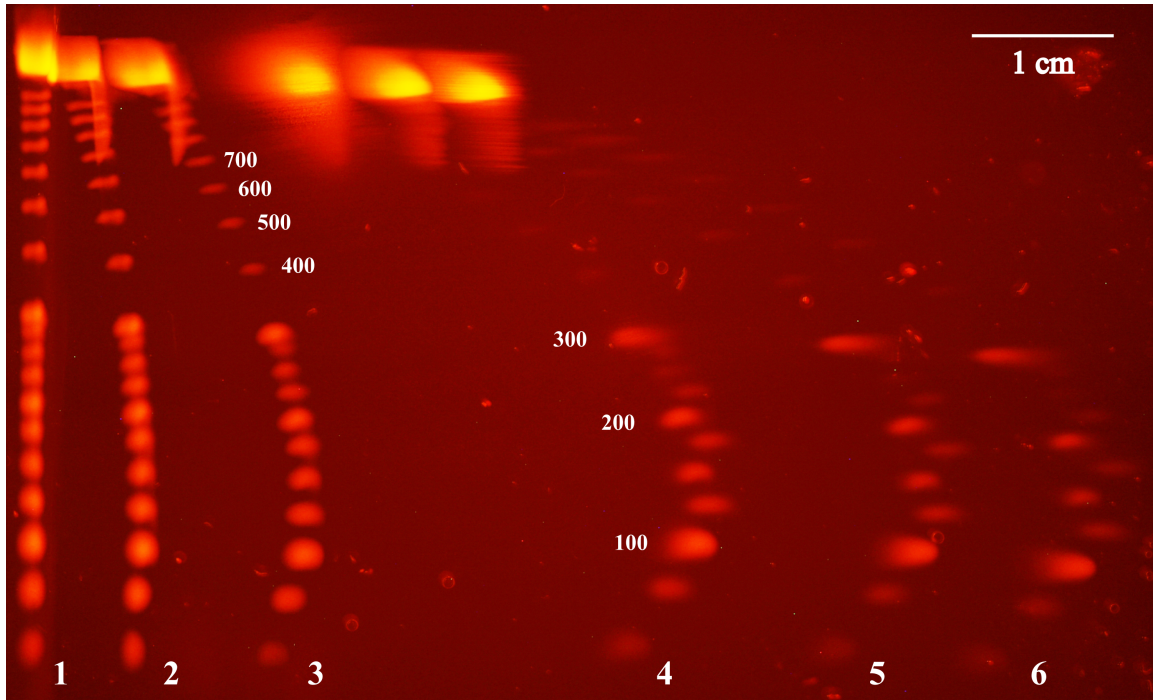

FIG. 4. The 2DE result of the 25 bp and 100 bp DNA ladders progressing from left to right in 24% pluronic F127. The 100, 200 and 300 bp fragments are 2 - 3 times brighter than the others due to the addition. The left-most (first) column shows the initial status of the DNA fragments separated by size in 2.5% agarose gel. The DNA bands moved through the pluronic gel from the second column to the sixth column. The scale bar is 1 cm in length.

Figure 5 shows the 2DE results of the 10 bp DNA ladder in 24% pluronic F127 gels. The 10 bp DNA ladder provides a narrower spacing between bands than the 25 bp DNA ladder, so that it can be very useful to investigate the zig-zag pattern. The left column in each subfigure was photographed shortly after all bands had entered the pluronic gel, and the right column was photographed after electrophoresing for about 14 hours. Surprisingly, the 20 bp band moves faster than the 30 bp band. The mobility increases from the 30 bp band to the 70 bp band, decreases from the 70 bp band to the 90 bp band, and then increases again from the 90 bp band to the 120 bp band. Longer DNA bands (> 100 bp) show the oscillatory pattern, but the individuals are not distinguishable.

Figure 5(b) shows the 2DE results of the same 10 bp DNA ladder used in Figure 5(a). The difference is that the separated DNA bands are trimmed off to include DNA bands ranging from 70 bp up to 300 bp and having a wider gap between adjacent bands. Similarly, longer DNA bands exhibit the oscillatory pattern. The peaks are 120 -130, 170 - 180, and 220 - 230 bp bands, and the troughs are 150, 200 and 250 bp bands. These are consistent with the values of peaks and troughs obtained from the 25 bp DNA ladder.

(a)
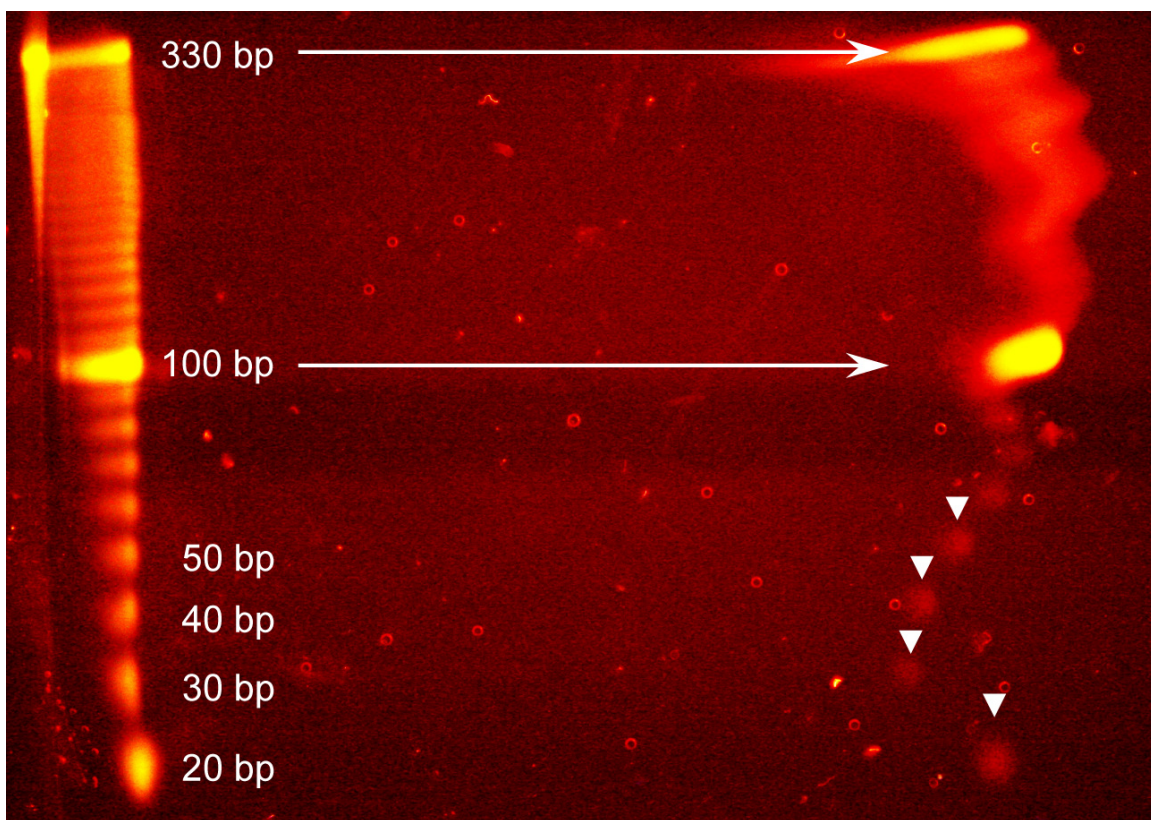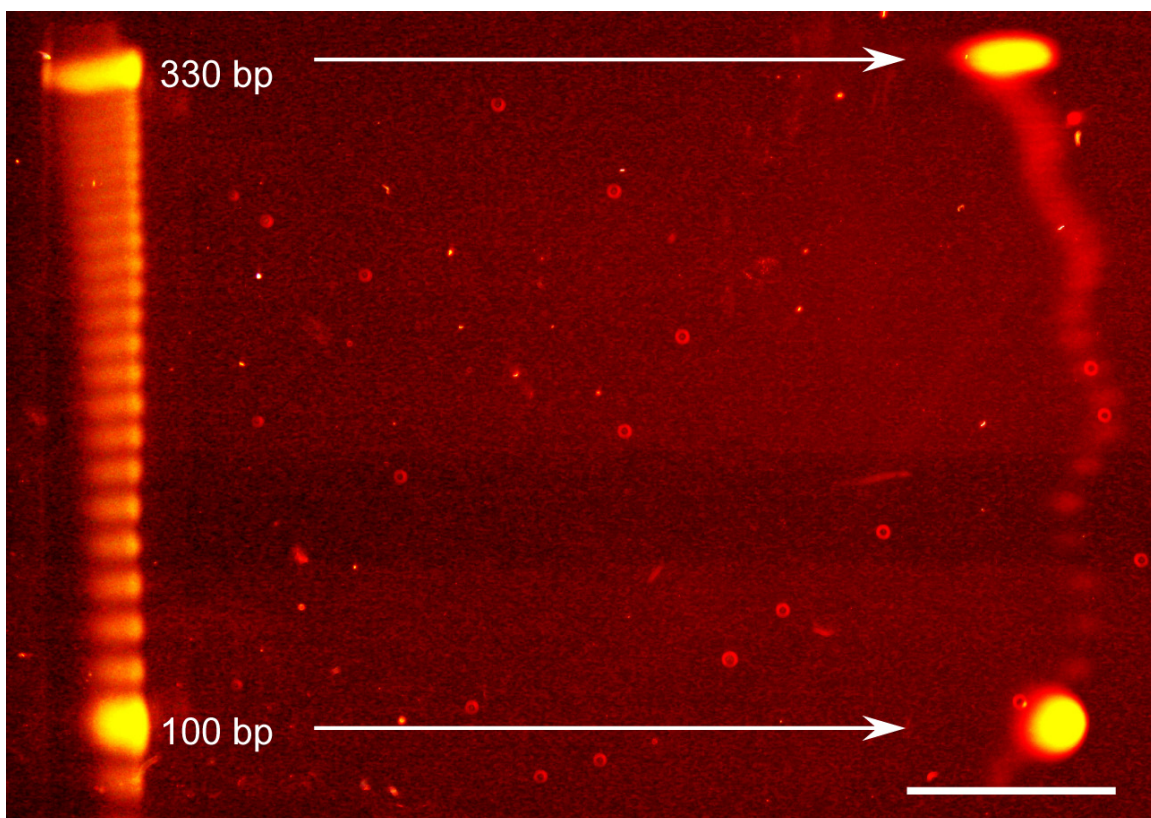
FIG. 5. The 2DE results of the 10 bp DNA ladder in 24 % pluronic F127. (a) The 10 bp DNA ladder is initially separated in 3% agarose gel, and moves through the pluronic gel in the direction of arrows. Down-pointing cursors locate the final position of 20 to 50 bp bands. (b) A better resolution of the 10 bp DNA ladder ranging from 90 to 330 bp. After the bands are separated in 2.5% agarose gel, the propagated bands oscillate at the period of about the micellar diameter. The scale bar is 1 cm in length.

Figure 6 shows the mobility of DNA ladders in different concentrations (22, 24, 26, and 30%) of pluronic F127 gels. The mobility of the 20 bp fragment is higher than the 25 bp fragment, and is comparable to the mobility of the 400 bp fragment at all gel concentrations. The 20 bp DNA molecules are about 6.8 nm in length, which is shorter than the radius of the micelles (9 nm), while the 25 bp DNA molecules are about 8.5 nm in length. The mobility increases with increasing DNA length in the range of 30-175 bp, reaching a maximum at about 175 bp, and then decreases with DNA length. For DNA molecules longer than 2500 bp, the mobility saturates to a nonzero plateau value. Overlaid on these broad trends is a sinusoidal variation, with a periodicity that roughly corresponds to the micellar diameter (18 nm).
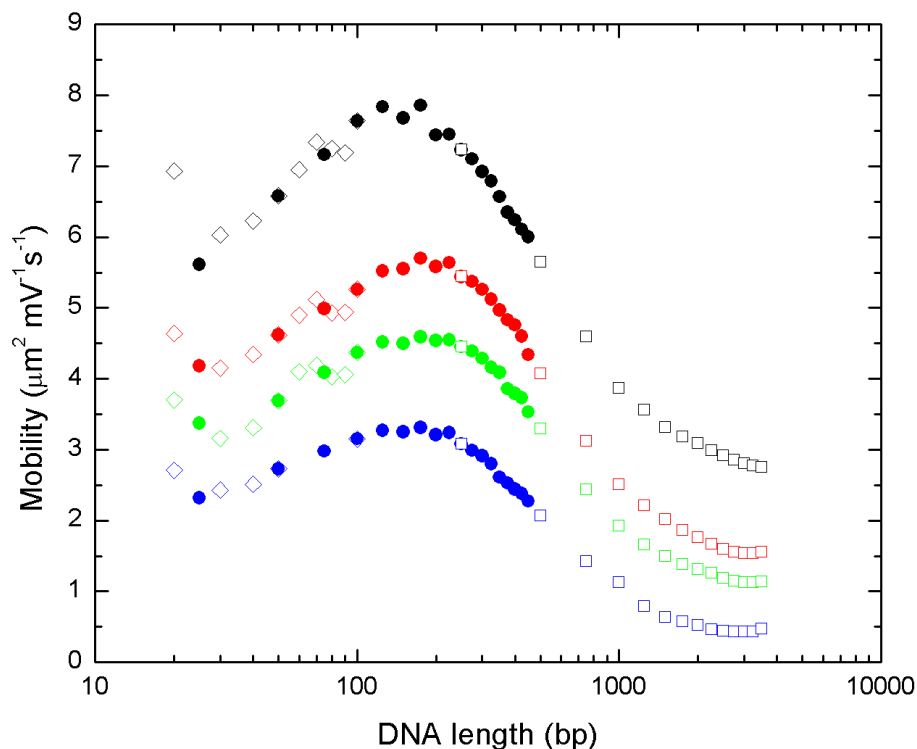

FIG. 6. The mobility of 10, 25, and 250 bp DNA ladders in 22%, 24%, 26%, and 30% (from top to bottom) pluronic F127 gels. The diamond open dots are the mobility of the

10 bp DNA ladder, the circular solid dots are the mobility of the 25 bp DNA ladder (Invitrogen), and the square open dots are the mobility of the 250 bp DNA ladder.

The electrophoretic mobility of DNA fragments in 10 bp and 25 bp DNA ladders is measured in 35% (w/v) pluronic P123 [Fig. 7(c)] under a DC field of 6 V/cm at room temperature. The length-dependent mobility in pluronics P123 and F127 share common features, even though they have different micellar dimensions [23,34]. For very short DNA molecules, there is a general rising trend in mobility as a function of DNA length. The monotonic decrease of mobility with DNA length for long DNA molecules ($L > 150$ bp) qualitatively agrees with the mobility behaviors in pluronic F127 [22] and conventional polymer gels [27,28] that were previously reported. The mobility oscillates as a function of DNA length in the intermediate regime, exhibiting two maxima respectively at 50 bp and 100 bp, the difference between which corresponds to 17 nm in length.
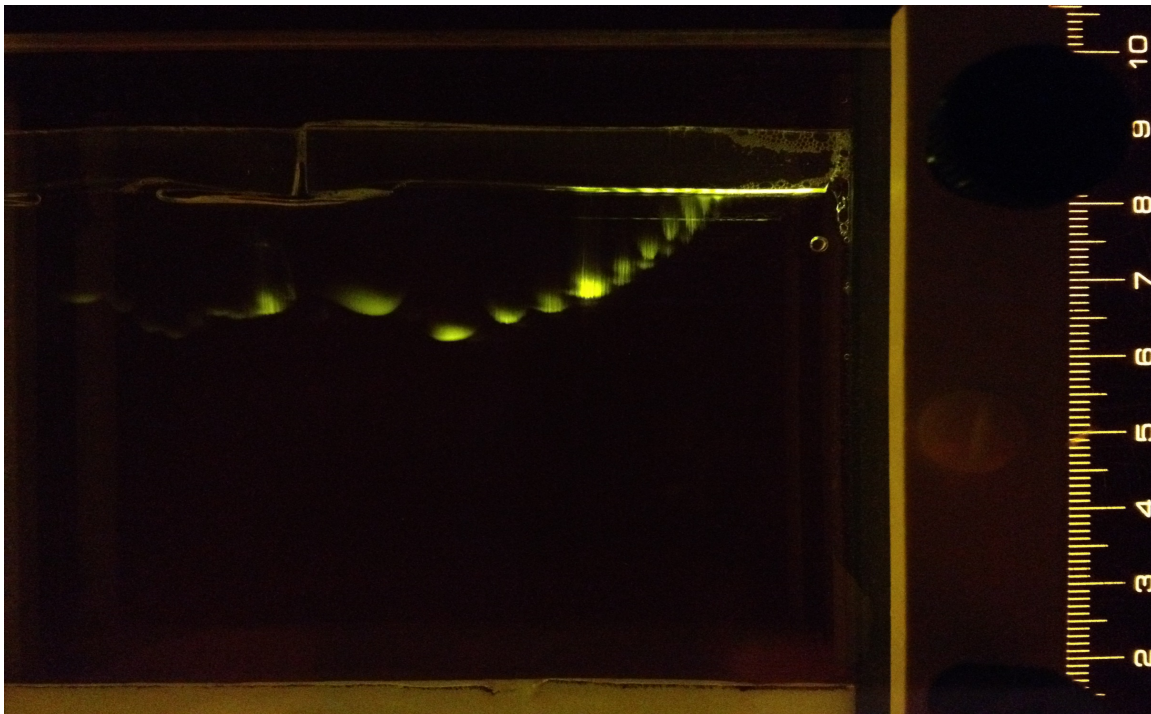

(a) 1.5 h
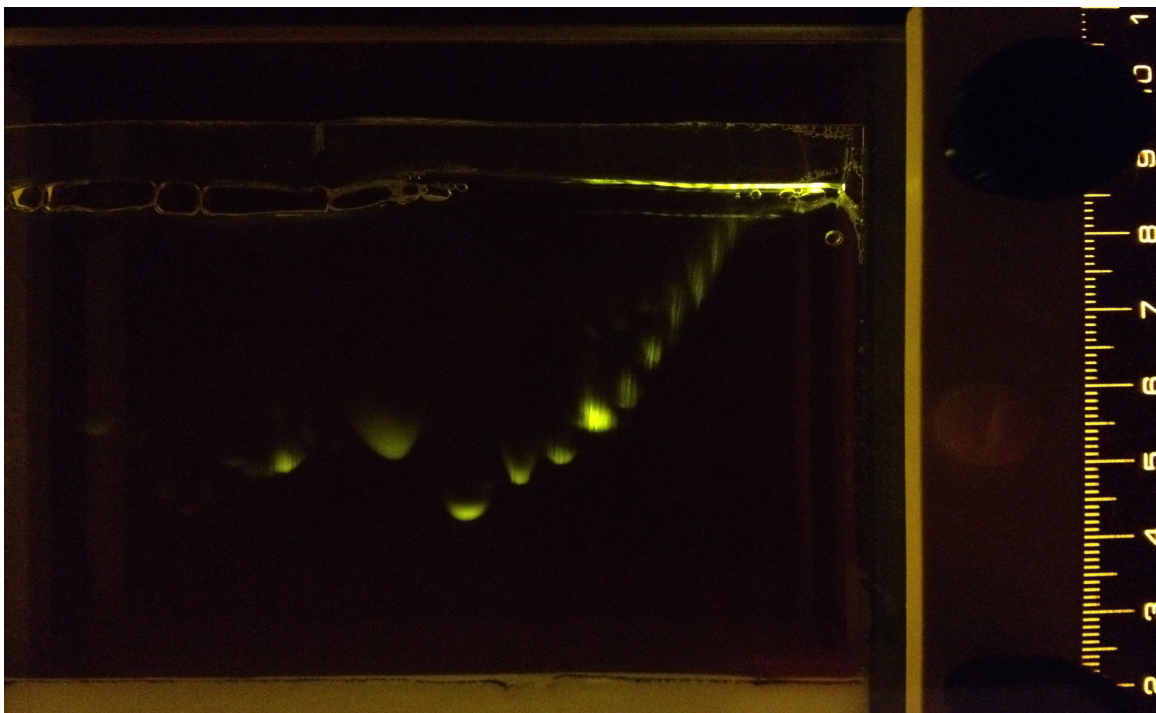
(b) 3.5 h
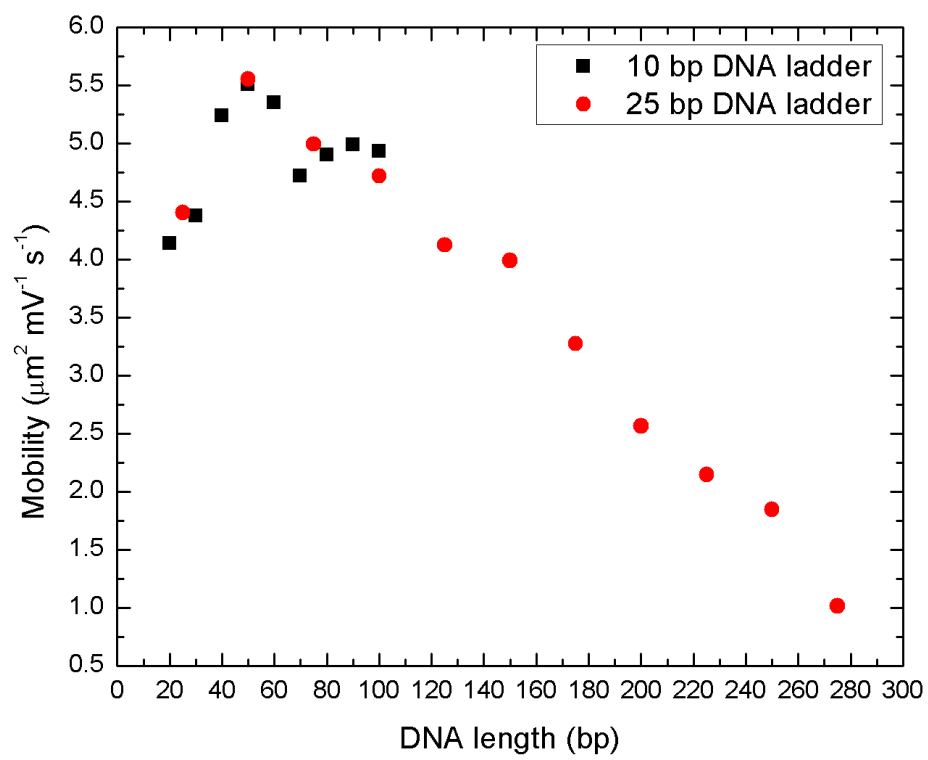
(c)

FIG. 7. Fluorescent images of separated DNA ladders and their electrophoretic mobility measured in pluronic P123.

B. BD simulations of DNA migration in pluronic lattice

Figure 8 shows the simulated mobility vs. DNA length in pluronic F127 [$R_m = 9.0$ nm, $R_c = 4.5$ nm, Fig. 8(a)] and P123 [$R_m = 8.1$ nm, $R_c = 5.7$ nm, Fig. 8(b)] lattices, under an electric field of 1 kV/cm. The mobility increases with DNA length for very short strands ($\leq 40\text{-}50$ bp), primarily due to the short-ranged hydrodynamic interactions. For longer DNA molecules, the attenuation of hydrodynamic coupling between segments farther apart (>100 bp) and entanglement with PEO polymers ($L > l_e$), result in the decreased mobility with increasing DNA length. The rising and falling trends of length-dependent mobility in face-centered-cubic lattices qualitatively agree with the experimental measurements in pluronic F127 (Fig. 6) and P123 [Fig. 7(c)] gels under a much weaker electric field. Moreover, the simulated mobility shows some oscillations with DNA length, which captures part of the oscillating features observed in experimental measurements.
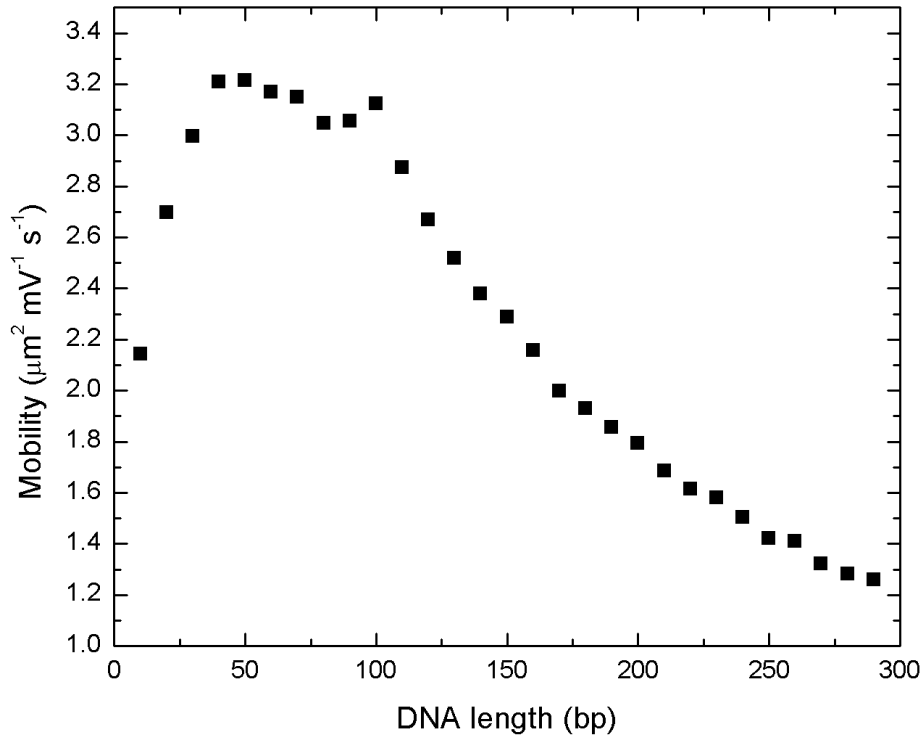
(a)
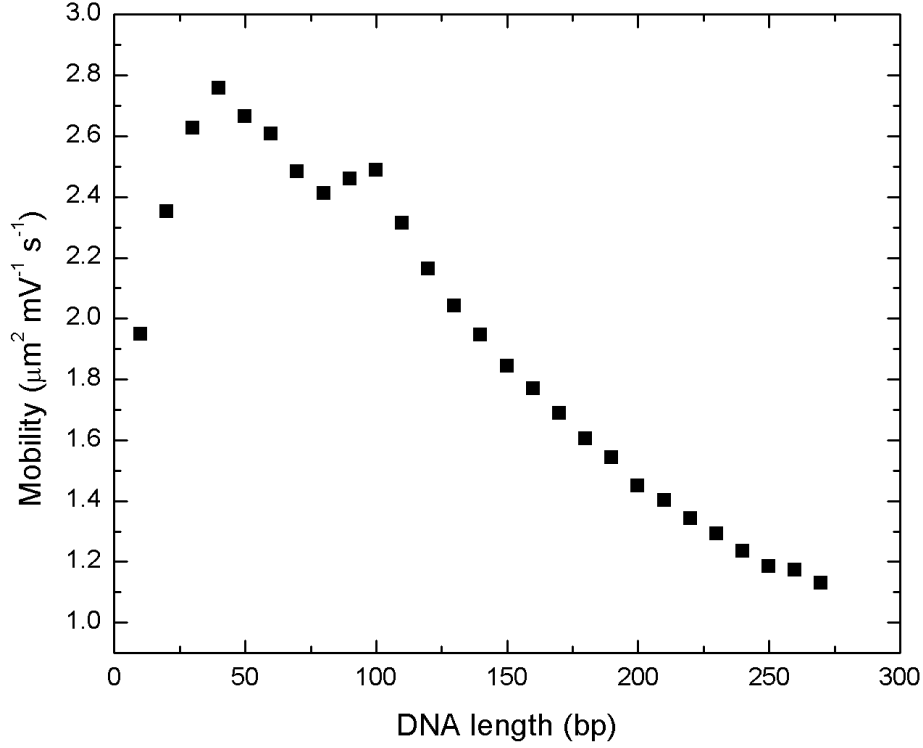
(b)

FIG. 8. Mobility vs. DNA length in pluronic (a) F127 and (b) P123 lattices computed from Brownian dynamics simulations. The error bars, which are smaller than the symbols, are from the standard errors of 50 independent runs.

Three key mechanisms are incorporated in the Brownian dynamics simulations, i.e., hydrodynamic interactions, repulsion from micelles and entanglement between DNA and PEO chains. In order to test the importance of each mechanism, we performed additional simulations by turning off hydrodynamic interactions, repulsion or entanglement (Fig. 9), and compared the results with the data shown in Figure 8.
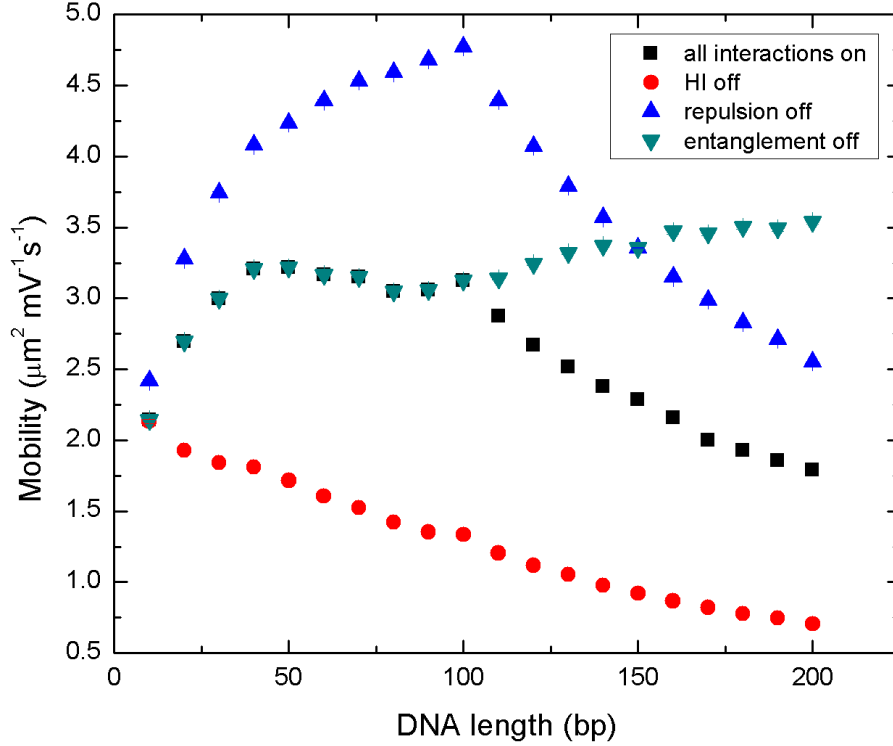
FIG. 9. Mobility vs. DNA length in pluronic F127 lattice, with hydrodynamic interactions, repulsion or entanglement being turned off in Brownian dynamics simulations. The applied electric field is 1 kV/cm. The error bars are from the standard errors of 50 independent runs.

Without hydrodynamic interactions, the mobility decreases monotonically with DNA length, so the initial rise of mobility as shown in Figure 6 is not reproduced. If the repulsive force from micelles is turned off, the overall mobility gets enhanced, meanwhile, the non-monotonic variation of mobility vs. DNA length at ~75 bp vanishes. The repulsive force from micelles strengthens the complex internal structure of pluronic gels, so that DNA could sense the geometries better, which is indirectly suggested by the first peak (~50 bp) in mobility vs. DNA length plot [Fig. 8(a)]. When the entanglement between long DNA molecules and PEO chains is not incorporated in the model, due to the predominant intra-DNA hydrodynamic interactions over the length scale of a ~100 bp segment, the mobility keeps increasing with DNA length, but at a lower rate in comparison with short DNA molecules. The monotonically decreasing trend of mobility with DNA length at higher molecular weights is not reproduced if the entanglement is turned off. In summary, the hydrodynamic interaction and entanglement lead to the rise and fall of mobility with DNA length, respectively; the repulsion brings the non-monotonic variations of mobility with DNA length, when the DNA length is comparable to the micellar dimension (~18 nm). When all the three mechanisms are incorporated simultaneously, a qualitative agreement with experimental measurements is achieved.

C. MD simulations of DNA migration in pluronic lattice

Two qualitative hypotheses are proposed to explain the initial rise in mobility, namely (i) an entropy induced chromatographic effect, and (ii) a hydrodynamic effect, in which DNA segments self-organize to lower the effective drag. In the BD simulations, micelle cores are impenetrable to DNA molecules, and micelle coronas are implicitly modeled using the repulsive elastic force (Eq. 3) and diffusion tensor (Eq. 4). This model seems to semi-quantitatively capture the rise and fall in mobility with DNA length. This would seem to favor the hydrodynamic effect hypothesis. However, it should be recognized that due to the implicit treatment of the micelle coronas, it is not possible to directly test the validity of the "chromatographic effect" hypothesis using these simulations. Furthermore, it can be argued that hydrodynamic interactions, especially as they are applied in simulations of dilute polymer solutions, should be screened out in the crowded microenvironment of the pluronic gels. The maximum separation of the PEO chains is about 2 nm at the edge of micelles and less than 2 nm in the vicinity of micelle cores, which is well within the semi-dilute regime, where we expect the hydrodynamic interactions to be unimportant. These hypotheses and issues cannot be resolved by modeling the micelle coronas implicitly. Therefore, we performed coarse-grained molecular dynamics simulations by explicitly modeling the PEO polymers as beads connected by springs. The simulation methods are described in details in Appendix B.

1. DNA length-dependent mobility in pluronic lattice

Figure 10 shows the average velocity of the DNA molecules as a function of DNA length in pluronic F127 lattice ($R_m = 9.0$ nm, $R_c = 4.5$ nm). The applied electric field is 25 kV/cm along [100] direction. The velocity v, which is proportional to the mobility, initially increases, reaches a maximum around 150 bp, and then decreases as the length of the DNA increases. Thus, the non-monotonicity observed in the experiments is captured in the MD simulations of the toy system. In addition, we artificially increased the stiffness of the DNA by increasing the bending energy k_{bend} ten-fold, so that the persistence length is 500 nm. The stiffer DNA also shows a characteristic initial increase in the mobility as a function of DNA length up to 100 bp, and decreases thereafter, which is punctuated by local maxima. We expect the stiffer DNA to be more sensitive to the set of length-scales that characterize the pluronic gel.
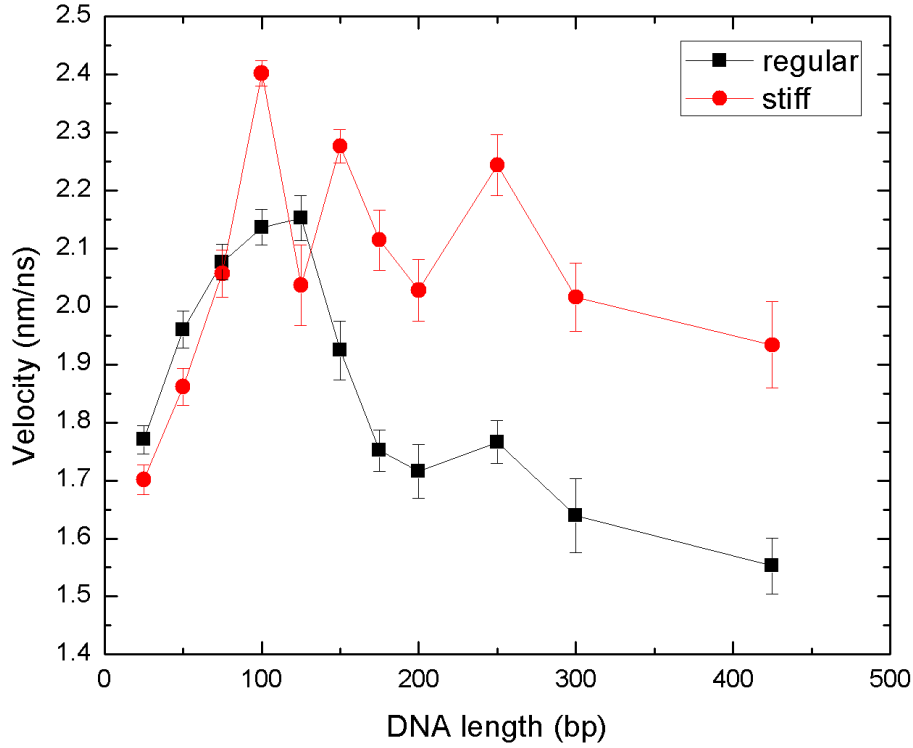
FIG. 10. Velocity vs. DNA length in pluronic F127 lattice computed from molecular dynamics simulations. The error bars are from the standard errors of 20 independent runs.

2. Exclusion of chromatographic effect in pluronic matrix

In order to check whether the initial rise of mobility as a function of DNA length is due to chromatographic effect, the average distance between the center of mass (com) of a DNA molecule and the closest micelle core is evaluated (Fig. 11). If the chromatographic effect were in force, one would expect the shorter DNA molecules to migrate closer to the micelle cores than longer DNA molecules. However, we do not observe any such trend in Figure 11. The average com-to-core distance varies slightly for both regular [Fig. 11(a)] and stiff [Fig. 11(b)] DNA molecules, but is roughly a constant for DNA molecules with different contour lengths in each case. The DNA chains are pushed away from micelle cores towards the periphery due to steric repulsion, which arises naturally in these MD simulations by explicitly representing the PEO polymers. These results rule out the chromatographic effect as a possible cause to the initial rise of mobility with DNA length.
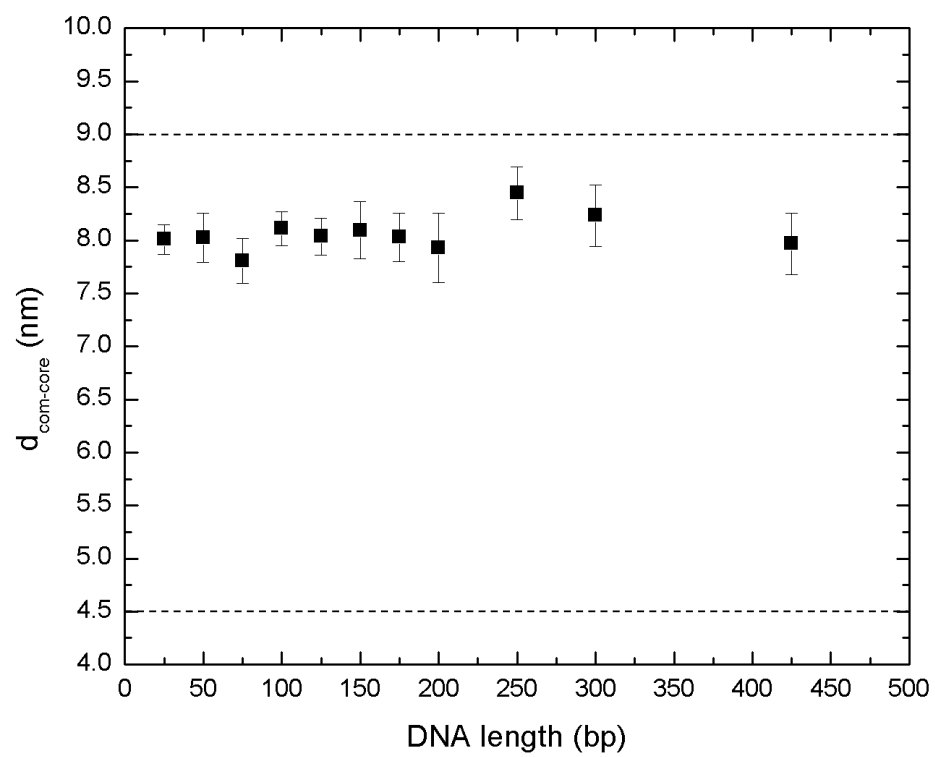
(a)
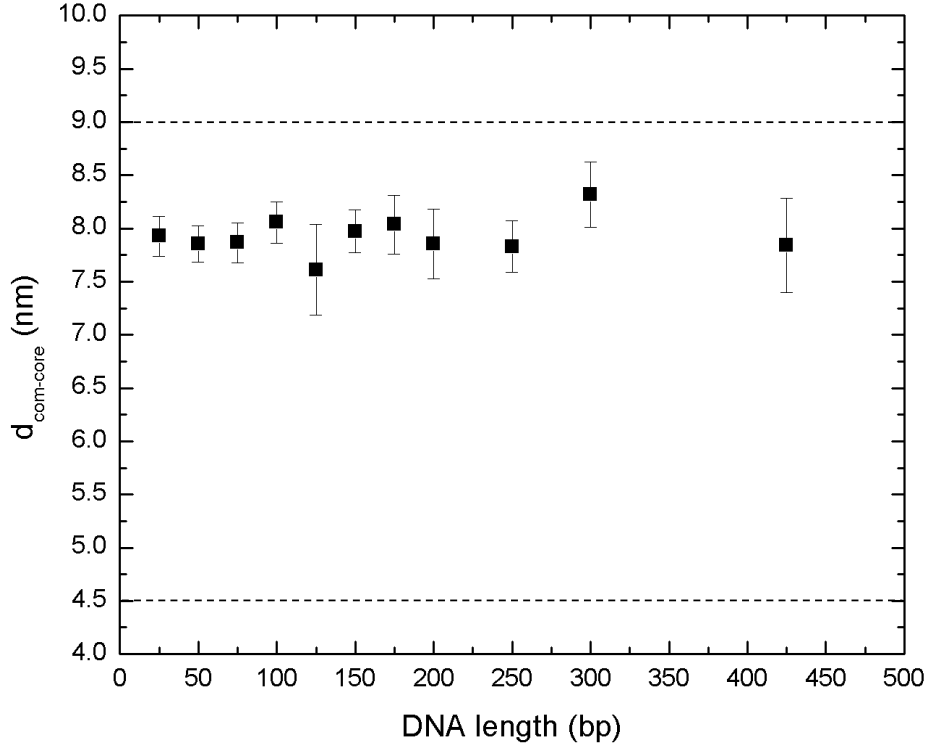
(b)

FIG. 11. The average distance from the center of mass (com) of the DNA molecules to the closest micelle cores for (a) regular and (b) stiff DNA molecules. The error bars are from the standard errors of 20 independent runs. The dashed lines correspond to the radii of micelles ($R_m = 9.0$ nm) and micelle cores ($R_c = 4.5$ nm).

3. Interpretation of hydrodynamic interactions in pluronic matrix

Brownian particles moving in fluids exhibit long-ranged hydrodynamic coupling by generating and responding to perturbations in the local velocity field. In a general sense, this velocity field arises purely from the motion of solvent molecules. The microenvironment in hydrogels is completely different from that in free solutions, where the presence of gel fibers leads to a fast decay of hydrodynamic interactions on the length scale of the macromolecules. As for electrophoresis in pluronic liquid crystals, micelles are closely packed and there is limited space for DNA molecules to travel through. In addition, poly(ethylene oxide) polymers mounted on micelle cores also screen the local velocity field to a large extent. Therefore, the hydrodynamic coupling mediated by solvent is probably not valid in the case of pluronic gels. However, any decrease in the friction per DNA segment due to collective polymer behaviors mediated by the environment may be categorized under a broader conceptualization of hydrodynamic interaction.

Specifically, careful observation of MD trajectory data suggests that as the leading DNA bead is propelled in the electric field direction, it pushes apart PEO polymers and forges a path for the subsequent beads. Since these beads can slide through the opening in PEO polymers created by the leading bead, it effectively reduces the drag force that they experience. This mode of hydrodynamic coupling is analogous to the usual understanding of hydrodynamic interactions in fluids, in the sense that a particle perturbs the local velocity field while moving and the surrounding particles respond to the perturbation. The key difference is that the medium through which perturbations propagate is comprised of a complex structured fluid (hydrated PEO polymers), rather than pure solvents as in dilute polymer solutions.

Due to Brownian forces and the presence of geometric obstacles, the DNA contour does not trace the path of the leading bead exactly. Indeed, sometimes the DNA flips over, and the identity of the leading bead itself does not remain unchanged throughout the simulation. However, it is possible to quantify the 'hydrodynamic interactions' between DNA segments by tracking how closely the trajectories of different beads bunch up. In other words, we can try to estimate the average diameter of the tube in which trajectories of all the beads are confined. The long axis of this tube aligns roughly in the field direction, and its width approximately represents the hydrodynamic diameter,

$$\overline{D} = \sqrt{D^2} \sim 2R_H. \tag{6}$$

According to the Rouse model [52], where each DNA bead is subjected to a random thermal force and a drag force, the drag experienced by a DNA chain is proportional to its contour length,

$$\zeta_{chain}^R \sim N\zeta_0, \tag{7a}$$

where N is the total number of beads on the chain, and ζ_0 is the drag per bead. By including the hydrodynamic interactions mediated by solvent, the drag experienced by a chain is given by the Zimm model [53],

$$\zeta_{chain}^Z \sim \eta R_H, \tag{7b}$$

where η is the viscosity of the solvent. By comparing the drag force calculated from Rouse and Zimm models, the importance of intra-molecular hydrodynamic coupling can be evaluated,

$$\frac{\zeta_{chain}^Z}{\zeta_{chain}^R} \sim \frac{R_H}{N} \sim \frac{\overline{D}}{N}. \tag{7c}$$

$\overline{D}/N$ is a measure of the average drag per segment on a DNA chain.

Piecewise linear reconstruction of trajectories was carried out first by projecting $r_j(t_k)$, the coordinate of bead j at time t_k, onto the piecewise linear trajectory of bead i, and $d_{ij}(t_k)$ was obtained as the shortest distance from bead j at time t_k to the

trajectory of bead i. The same calculations were performed for each snapshot of bead j, and the sum of the distance squared of n snapshots is denoted as D_{ij}^{2},

$$D_{ij}^{2} = \sum_{k=1}^{n} d_{ij}^{2}\left(t_k\right). \tag{8a}$$

The hydrodynamic diameter $\overline{D}$ was calculated by averaging D^2 over all pairs of beads on the chain,

$$\overline{D} = \sqrt{\frac{1}{N}\left\{\frac{1}{N-1}\left[\sum_{\substack{i,j=1 \\ i\neq j}}^{N} D_{ij}^{2}\right]\right\}}. \tag{8b}$$

$\overline{D}/N$ vs. DNA length ($\sim N$) for both regular and stiff DNA molecules is plotted in Figure 12.
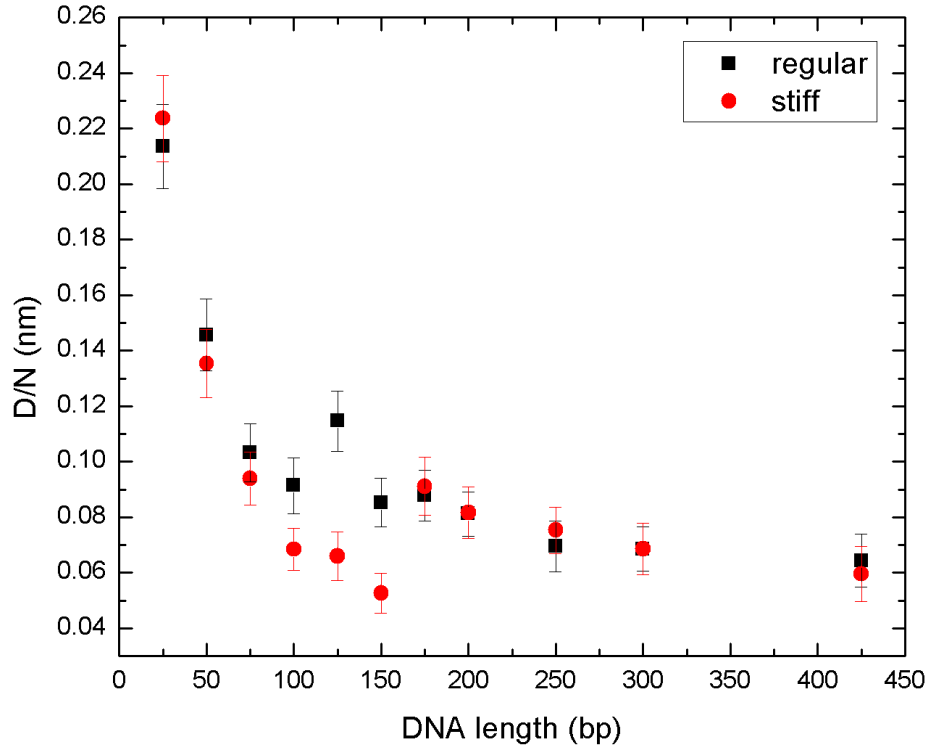

FIG. 12. $\overline{D}/N$ vs. DNA length for regular and stiff DNA molecules in pluronic F127 lattice. The error bars are from the standard errors of 20 independent runs.

The average drag per bead decreases rapidly as a function of the contour length up to approximately 100 bp, after which it reaches a plateau. The decrease in the drag force, via a reduced hydrodynamic diameter, is a manifestation of the intra-molecular

hydrodynamic coupling. The effectiveness of hydrodynamic coupling for DNA molecules up to 100 bp long is consistent with the assumption in Brownian dynamics simulations where hydrodynamic interactions are attenuated beyond the length scale of a 100 bp DNA segment.

The MD simulations confirm again the importance of hydrodynamic interactions in regulating DNA migration in pluronic matrices. This type of hydrodynamic interactions should be interpreted as the coupling mediated by the surrounding PEO polymers, instead of the solvent itself.

IV. CONCLUSIONS

In summary, the electrophoretic motion of DNA molecules is non-monotonic with respect to their size in pluronic gels. In pluronic F127, generally, for small sizes, there is an increase in mobility with length up to about 175 bp; for longer DNA, the electrophoretic mobility decreases exponentially and reaches a non-zero limit at about 2500 bp. Superposed on this overall dependence is a modulation of the mobility on a length scale corresponding to the diameter of the close packed micelles through which the DNA is migrating. A similar mobility behavior was also obtained in pluronic P123. Brownian dynamics and molecular dynamics simulations were performed to numerically calculate the DNA mobility in pluronic matrices under strong electric fields, the results of which are in qualitative agreement with each other as well as with the experimental measurements. Hydrodynamic interactions, rather than chromatographic effect, were justified as the primary reason for the initial rise of mobility as a function of DNA length. The non-monotonic variations of mobility vs. DNA length are possibly originated from the periodic crystal structures of pluronic gels. As for long DNA molecules, due to the entanglements with PEO polymers, their mobility monotonically decreases with length.

Although some details in the experimental data were not exactly reproduced by BD or MD simulations, results and additional analysis from simulations present a clear picture of the electrophoretic migration of short DNA molecules in pluronic liquid crystals. The dominant physical interactions, which lead to the unusual DNA length-dependent mobility, were revealed by the numerical simulations. Electrophoresis of duplex DNA molecules in micelle-packed crystal gels is a complex dynamic process. This study will contribute to an enhanced understanding of the dynamics of DNA molecules in pluronic gel and facilitation of pluronic gel as an alternative sieving medium for electrophoresis in the fields of molecular biology and biotechnology.

ACKNOWLEDGMENTS

APPENDIX A: ELECTROPHORETIC MOBILITY IN AGAROSE GELS

We measured the electrophoretic mobility of DNA fragments in 10 bp and 25 bp DNA ladders in 3% (w/v) agarose gels (Fig. A1). The mobility in agarose gels monotonically decreases with increasing DNA length in the range of 20-500 bp, which is different from the non-monotonic mobility behaviors in pluronic gels.
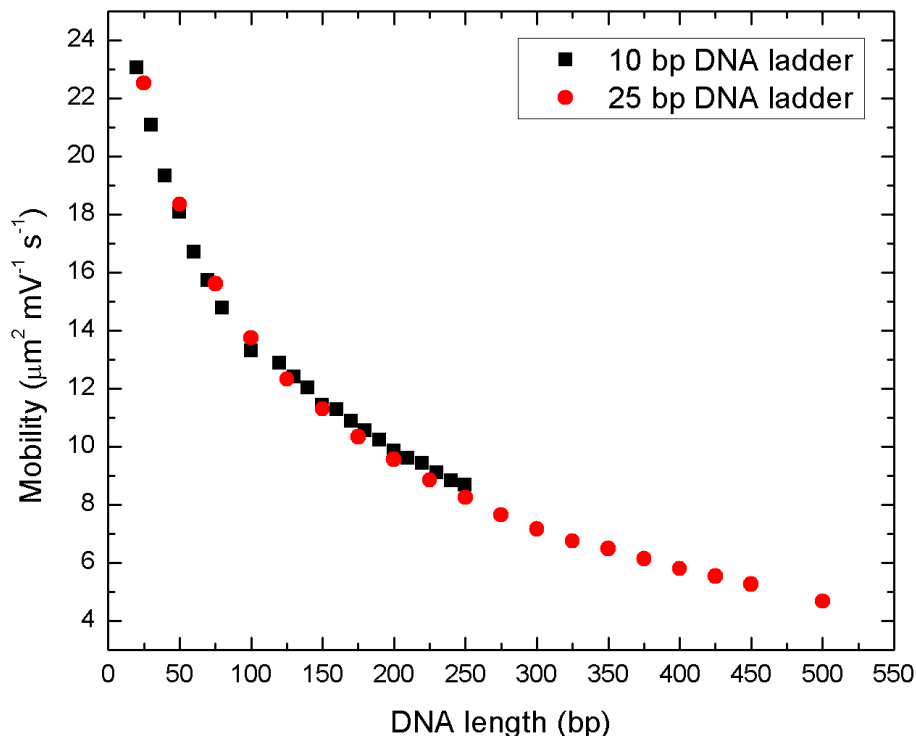

FIG. A1. The electrophoretic mobility of 10 bp and 25 bp DNA ladders in agarose gels (3% (w/v), 1×TBE). The applied electric field was 3.3 V/cm.

APPENDIX B: MD SIMULATION METHOD

We performed molecular dynamics (MD) simulations of DNA electrophoresis on toy system with the goal of qualitatively understanding the origin of the non-monotonic variation in mobility. The toy system was designed to resemble the pluronic F127; hairy nanoparticles, each consisting of an impenetrable PPO core, and surrounded by 36 PEO hairs, were arranged on a face-centered-cubic lattice. For computational efficiency, the number of PEO hair in the toy system was chosen to be only a quarter of the number of hair in the pluronic system.

The PEO hair and the DNA molecule were represented as bead-spring polymers. The repulsion between these beads is modeled by the shifted Weeks-Chandler-Andersen (WCA) potential,

$$U_{LJ}(r) = 4\varepsilon\left[\left(\frac{\sigma}{r}\right)^{12} - \left(\frac{\sigma}{r}\right)^{6}\right], r < 2^{1/6}\sigma, \tag{B1}$$

where $\sigma = 1$ nm, $\varepsilon = 2.5$ kJ/mol. Finite extensible nonlinear elastic (FENE) springs are used to model the connectivity of PEO hair and the DNA,

$$U_{FENE}(r) = -\frac{1}{2}k_{FENE}R_0^2\ln\left[1 - \left(\frac{r}{R_0}\right)^2\right], \tag{B2}$$

with $k_{FENE} = 30\varepsilon/\sigma^2$, and $R_0 = 1.7\sigma$. The dimensionless temperature is set to $k_B T/\varepsilon = 1$, which corresponds approximately a temperature of 300 K. Each individual PEO hair is represented by 17 beads, which corresponds to a contour length of approximately 27 nm. For the DNA, each bead represents 5 bp, which gives it a mass of approximately $m = 3250$ g/mol. The timescale based on the Lennard-Jones (LJ) units is $\tau = \sqrt{m\sigma^2/\varepsilon} \approx 36$ ps.

The repulsion between PPO cores is also represented by a WCA potential with energy scale ε and length-scale equal to its diameter 9σ. The interaction between the PPO cores and the DNA/PEO beads is modeled by a shifted-LJ potential,

$$U_{sLJ}(r) = 4\varepsilon\left[\left(\frac{\sigma}{r-\Delta}\right)^{12} - \left(\frac{\sigma}{r-\Delta}\right)^{6}\right], r < 2^{1/6}\sigma + \Delta, \tag{B3}$$

with $\Delta = 5\sigma$. The bending rigidity of the DNA molecule is modeled by a squared cosine form,

$$U_{bend} = k_{bend}\left[\cos\theta - \cos\theta_0\right]^2, \tag{B4}$$

with $k_{bend} = 275.35\varepsilon$ and $\theta_0 = \pi$ radians. This choice gives the DNA molecule a persistence length of ~50 nm. Each PEO hair is tethered to the PPO core by a stiff harmonic spring,

$$U_{harmonic}(r) = 5\times10^5\varepsilon(r-5.7\sigma)^2 \qquad .$$

(B5)

A simulation box of dimensions $127.31\sigma \times 76.38\sigma \times 76.38\sigma$, with 180 hairy nanoparticles and a DNA molecule was equilibrated. The equilibration was carried out by isotropically compressing the simulation box from an expanded initial configuration, with no particle overlaps, to the target volume in which the distance between PPO cores was 18σ as observed in experiments. DNA molecules ranging from 25 bp to 425 bp were modeled.

A uniform electric field of $E = 1.0\left(k_B T / q\sigma\right)$ was applied, where $q = 10e^-$ is the charge per DNA bead. 20 independent simulations, each 32 ns long, were carried out with a time-step of $\delta t = 1.75 \times 10^{-3}\tau$. The position of the DNA molecule was periodically recorded, and the average velocity of the center-of-mass v was calculated. The applied electric field corresponds to ~25 kV/cm in real-units and is quite large; however, this provided a large enough driving force to the DNA molecule to reliably compute mobility in a reasonable time period. It was observed that $v \propto E$, when E was varied between $0.5\left(k_B T / q\sigma\right)$ and $2.0\left(k_B T / q\sigma\right)$.

APPENDIX C: FIELD-DEPENDENT ELECTROPHORETIC MOBILITY

1. Field intensity

Numerical computations of DNA mobility in polymer liquid crystals are expensive. In molecular dynamics simulations, the primary driver of computational cost is the explicit resolution of the PEO polymers. Similarly, the most expensive step in the Brownian dynamics simulations is the modeling of hydrodynamic interactions via the $3N \times 3N$ diffusion tensor. In order to make numerical simulations feasible, strong electric fields were used in both MD and BD simulations, to enhance the signal of the electrophoretic migration, against the backdrop of Brownian diffusion. However, a low field of 6 V/cm was applied in electrophoresis experiments. Although the field intensities employed in the simulations are much higher, the electrophoretic mobility inferred from the simulations (Fig. C1) is found to be approximately constant in the regimes investigated. For example, starting for extremely high electric fields in BD simulations, the DNA mobility decreases with decreasing field intensity, but reaches a plateau at approximately 1 kV/cm. This allows us to estimate the mobility at even lower fields by extrapolating these high-field calculations.
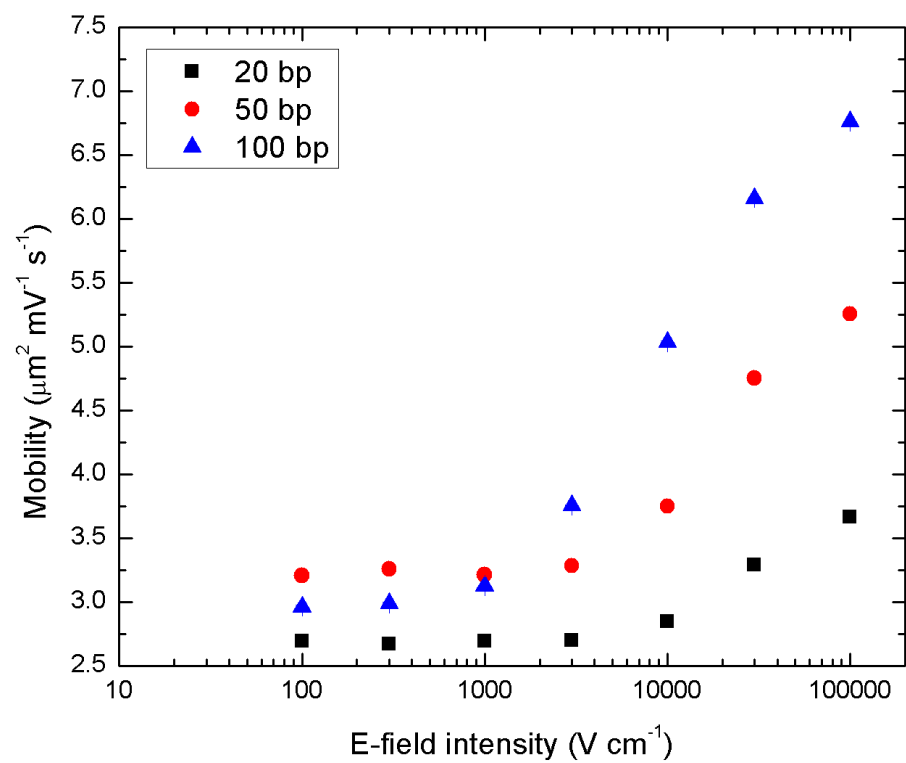
(a)
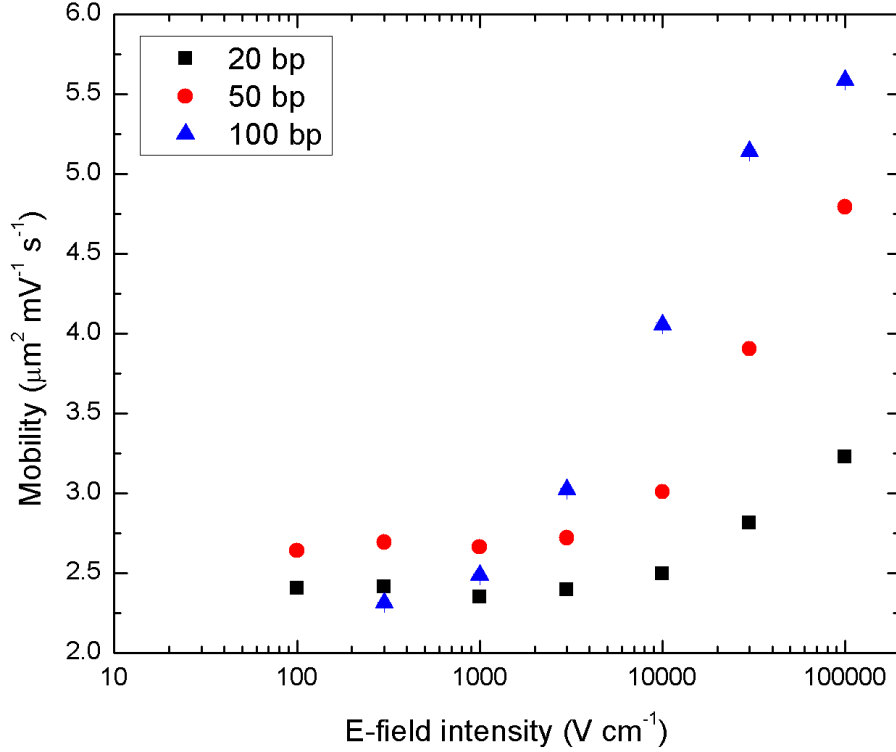
(b)

FIG. C1. Electric field intensity-dependent mobility of representative DNA molecules (20 bp, 50 bp and 100 bp) in pluronic (a) F127 and (b) P123 lattices computed from Brownian dynamics simulations. The electric fields are all in [100] direction with respect to the cubic lattices. All other simulation parameters are the same as in Figure 9. The error bars are from the standard errors of 50 independent simulations.

The Péclet number at different electric field intensities in Brownian dynamics simulations (pluronic F127) is calculated and summarized in Table C1. At electric fields of 1 kV/cm and lower, the Péclet number is less than 1, which indicates that simulations performed in this field range are not in the convection-dominated regime but a balance of convection and diffusion. The electrophoretic mobility calculated in this field range does not vary too much with field intensity (Fig. C1). At the electric field of 3 kV/cm, the Péclet number is on the order of 1, suggesting the transition to the convection-dominated regime, where the mobility starts to increase with field intensity as shown in Figure C1. At electric fields higher than 3 kV/cm, the DNA migration is in the convection-dominated regime (Pe>1), with the mobility monotonically increasing with field intensity (Fig. C1). Since DNA does not transport in convection-dominated regime under the electric field of 1 kV/cm and lower, these simulations are able to qualitatively resolve the migration mechanism and DNA length-dependent mobility in pluronic gels at even lower field intensity (e.g., 6 V/cm in electrophoresis experiments).

Table C1. Péclet number in pluronic F127 lattice.

DNA length (bp)	Péclet number						
	E=100 V/cm	E=300 V/cm	E=1 kV/cm	E=3 kV/cm	E=10 kV/cm	E=30 kV/cm	E=100 kV/cm
10	0.0034	0.0097	0.032	0.094	0.32	1.0	3.8
50	0.011	0.034	0.11	0.34	1.3	5.0	18
100	0.029	0.088	0.31	1.1	5.0	18	66
150		0.099	0.37	1.3	5.9	22	79
200			0.32	1.1	5.4	20	69
250			0.41	1.4	7.7	26	90
300			0.44		8.4	27	94

2. Field direction

In both pluronics F127 and P123, micelles are packed into face-centered-cubic structures under current electrophoresis conditions. Unlike in cross-linked polymer gels, the migration dynamics of DNA molecules in pluronic liquid crystals might be different along different field directions. In practice, bulk pluronic gels are composed of micelle-packed domains with various orientations. In numerical simulations, it is possible to compare the mobility of DNA molecules under electric fields orientated in specific directions. Brownian dynamics simulations in pluronic F127 and P123 lattices were performed (Fig. C2), under the electric field of 1 kV/cm in [110] or [111] direction with respect to the cubic lattices. In general, the mobility calculated under electric fields aligned in [110] and [111] directions is higher than in [100] direction. The enhancement of mobility under electric fields in [110] and [111] directions is more significant for relatively longer DNA molecules, which indicates that it might be easier for longer DNA chains to align with the field orientation in cubic lattices when the electric field is along certain preferred directions. Overall speaking, the DNA length-dependent mobility behaves consistently for three different field orientations, where the mobility increases and decreases with DNA length for short and long DNA molecules, respectively. In other words, the unusual length-dependent mobility primarily originates from the unique structures of pluronic liquid crystals formed by polymer micelles; the orientation of applied electric field plays a secondary role, and has only a modest effect on the mobility.
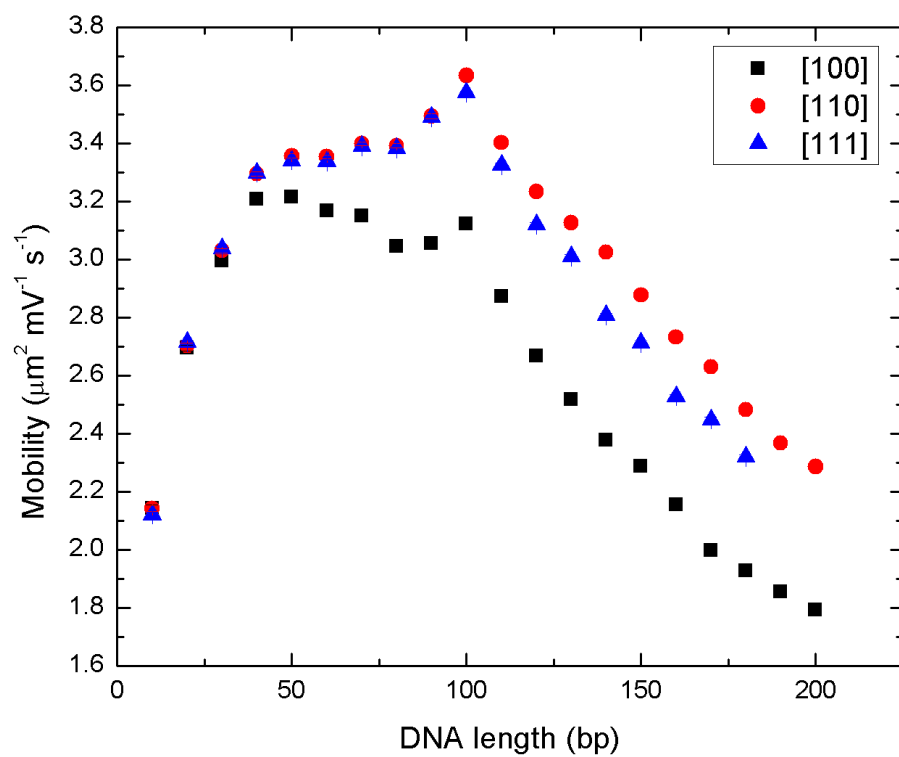
(a)
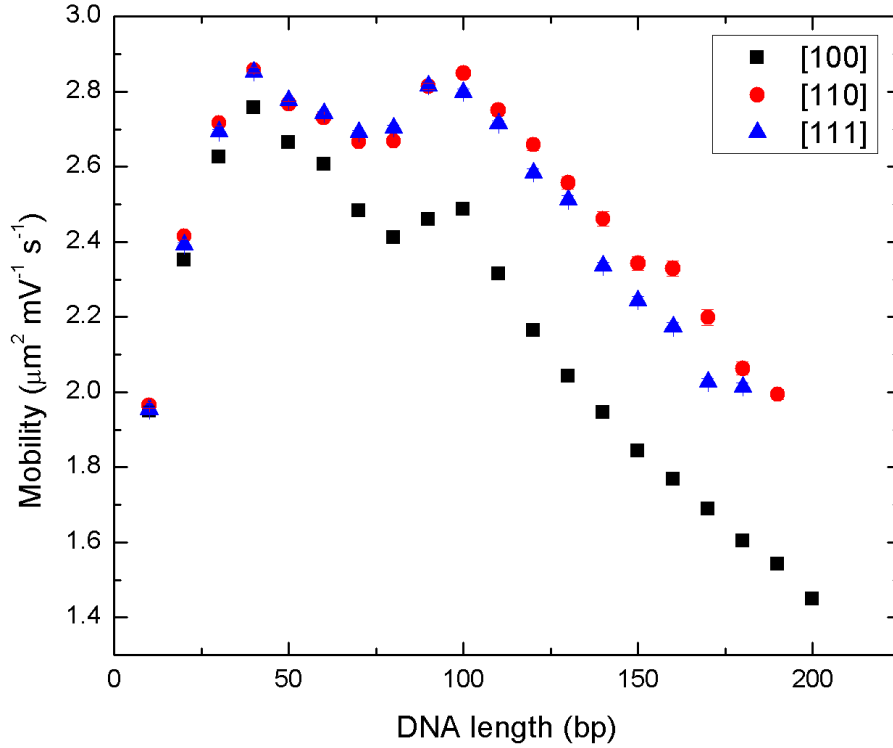
(b)

FIG. C2. DNA mobility in pluronic (a) F127 and (b) P123 lattices calculated from Brownian dynamics simulations. The electric field of 1 kV/cm is applied in [100], [110] or [111] direction with respect to the cubic lattices. All other simulation parameters are the same as in Figure 8. The error bars are from the standard errors of 50 independent simulations.

[1]   A. Tiselius, Trans. Faraday Soc. **33**, 524 (1937).

[2]   A. T. Woolley and R. A. Mathies, Anal. Chem. **67**, 3676 (1995).

[3]   E. M. Southern, J. Mol. Biol. **98**, 503 (1975).

[4]   J. C. Alwine, D. J. Kemp, and G. R. Stark, Proc. Natl. Acad. Sci. U. S. A. **74**, 5350 (1977).

[5]   H. Towbin, T. Staehelin, and J. Gordon, Proc. Natl. Acad. Sci. U. S. A. **76**, 4350 (1979).

[6]   D. J. C. Pappin, P. Hojrup, and A. J. Bleasby, Curr. Biol. **3**, 327 (1993).

[7]   W. J. Henzel, T. M. Billeci, J. T. Stults, S. C. Wong, C. Grimley, and C. Watanabe, Proc. Natl. Acad. Sci. U. S. A. **90**, 5011 (1993).

[8]   M. Mann, P. Højrup, and P. Roepstorff, Biol. Mass Spectrom. **22**, 338 (1993).

[9]   P. James, M. Quadroni, E. Carafoli, and G. Gonnet, Biochem. Bioph. Res. Co. **195**, 58 (1993).

[10]   J. R. Yates, S. Speicher, P. R. Griffin, and T. Hunkapiller, Anal. Biochem. **214**, 397 (1993).

[11]   A. Meller, L. Nivon, and D. Branton, Phys. Rev. Lett. **86**, 3435 (2001).

[12]   N. Pernodet, V. Samuilov, K. Shin, J. Sokolov, M. H. Rafailovich, D. Gersappe, and B. Chu, Phys. Rev. Lett. **85**, 5651 (2000).

[13]   C. F. Chou, R. H. Austin, O. Bakajin, J. O. Tegenfeldt, J. A. Castelino, S. S. Chan, E. C. Cox, H. Craighead, N. Darnton, T. Duke, and J. Han, Electrophoresis **21**, 81 (2000).

[14]   J. Han and H. G. Craighead, Science **288**, 1026 (2000).

[15]   J. Han, S. W. Turner, and H. G. Craighead, Phys. Rev. Lett. **83**, 1688 (1999).

[16]   P. S. Doyle, J. Bibette, A. Bancaud, and J. L. Viovy, Science **295**, 2237 (2002).

[17]   B. Tinland, H. Ren, C. Desruisseaux, L. C. McCormick, G. Drouin, and G. W. Slater, Electrophoresis **22**, 2424 (2001).

[18]   E. Southern, Methods Enzymol. **68**, 152 (1979).

[19]   T. Mamiatis, E. F. Fritsch, J. Sambrook, and J. Engel, *Molecular Cloning–A Laboratory Manual* (Cold Spring Harbor Laboratory, New York, 1982).

[20]   J. Narayanan, J. Y. Xiong, and X. Y. Liu, in *Journal of Physics: Conference Series, Vol. 28* (IOP Publishing, 2006), p. 83.

[21]   D. L. Holmes and N. C. Stellwagen, Electrophoresis **12**, 612 (1991).

[22]   R. L. Rill, B. R. Locke, Y. Liu, and D. H. Van Winkle, Proc. Natl. Acad. Sci. U. S. A. **95**, 1534 (1998).

[23]   C. Wu, T. Liu, B. Chu, D. K. Schneider, and V. Graziano, Macromolecules **30**, 4574 (1997).

[24]   S. You and D. H. Van Winkle, J. Phys. Chem. B **114**, 4171 (2010).

[25]   R. Svingen, P. Alexandridis, and B. Åkerman, Langmuir **18**, 8616 (2002).

[26] R. Svingen and B. Åkerman, J. Phys. Chem. B **108**, 2735 (2004).

[27] D. H. Van Winkle, A. Beheshti, and R. L. Rill, Electrophoresis **23**, 15 (2002).

[28] R. L. Rill, A. Beheshti, and D. H. Van Winkle, Electrophoresis **23**, 2710 (2002).

[29] A. Chrambach and D. Rodbard, Science **172**, 440 (1971).

[30] T. Maniatis, A. Jeffrey, and H. Van deSande, Biochemistry **14**, 3787 (1975).

[31] J. P. Habas, E. Pavie, C. Perreur, A. Lapp, and J. Peyrelasse, Phys. Rev. E **70**, 061802 (2004).

[32] C. Chaibundit, N. M. Ricardo, N. M. Ricardo, F. D. M. Costa, M. G. Wong, D. Hermida-Merino, J. Rodriguez-Perez, I. W. Hamley, S. G. Yeates, and C. Booth, Langmuir **24**, 12260 (2008).

[33] P. Alexandridis and L. Yang, Macromolecules **33**, 5574 (2000).

[34] R. Ganguly, V. K. Aswal, P. A. Hassan, I. K. Gopalakrishnan, and J. V. Yakhmi, J. Phys. Chem. B **109**, 5653 (2005).

[35] G. W. Slater, C. Holm, M. V. Chubynsky, H. W. de Haan, A. Dube, K. Grass, O. A. Hickey, C. Kingsbury, D. Sean, T. N. Shendruk, and L. Zhan, Electrophoresis **30**, 792 (2009).

[36] K. Grass, U. Böhme, U. Scheler, H. Cottet, and C. Holm, Phys. Rev. Lett. **100**, 096104 (2008).

[37] K. Grass and C. Holm, Farad. Discuss. **144**, 57 (2010).

[38] J. Boileau and G. W. Slater, Electrophoresis **22**, 673 (2001).

[39] N. Laachi, C. Declet, C. Matson, and K. D. Dorfman, Phys. Rev. Lett. **98**, 098106 (2007).

[40] Y. M. Lee and Y. L. Joo, J. Chem. Phys. **127**, 124902 (2007).

[41] A. Mohan and P. S. Doyle, Macromolecules **40**, 8794 (2007).

[42] K. D. Dorfman, Rev. Mod. Phys. **82**, 2903 (2010).

[43] J. Ou, J. Cho, D. W. Olson, and K. D. Dorfman, Phys. Rev. E **79**, 061904 (2009).

[44] C. D. Huang, D. Y. Kang, and C. C. Hsieh, Biomicrofluidics **8**, 014106 (2014).

[45] C. C. Hsieh, L. Li, and R. G. Larson, J. Nonnewton. Fluid Mech. **113**, 147 (2003).

[46] N. C. Stellwagen, C. Gelfi, and P. G. Righetti, Biopolymers **42**, 687 (1997).

[47]   R. K. Prud'homme, G. Wu, and D. K. Schneider, Langmuir **12**, 4651 (1996).

[48]   P. G. de Gennes, *Scaling Concepts in Polymer Physics* (Cornell University Press, 1979).

[49]   M. D. Graham, Annu. Rev. Fluid Mech. **43**, 273 (2011).

[50]   P. G. de Gennes, J. Chem. Phys. **55**, 572 (1971).

[51]   D. L. Ermak and J. A. McCammon, J. Chem. Phys. **69**, 1352 (1978).

[52]   P. E. Rouse Jr, J. Chem. Phys. **21**, 1272 (1953).

[53]   B. H. Zimm, J. Chem. Phys. **24**, 269 (1956).